Groundwater Monitoring&Remediation

Integrated Plume Treatment Using Persulfate Coupled with Microbial Sulfate Reduction

by Mahsa Shayan, Neil R. Thomson, Ramon Aravena, James F. Barker, Eugene L. Madsen, Massimo Marchesi, Christopher M. DeRito, Daniel Bouchard, Tim Buscheck, Ravi Kolhatkar, and Eric J. Daniels

Abstract

The integration or sequential use of different remediation technologies, also referred to as a combined remedy, has become an emerging strategy for the treatment of contaminated sites. Coupling chemical oxidation using persulfate with enhanced bioremediation (EBR) under sulfate reducing conditions is a plausible combined remedy. To characterize the role of the mass removal processes (e.g., chemical oxidation vs. sulfate reduction) and to quantify the impact of persulfate on indigenous microbial processes in a combined persulfate/EBR treatment system, a pilot-scale field experiment was conducted in a 24-m long sheet pile-walled gate over a period of approximately 400 d. After dissolved benzene, toluene, and *o*-xylene (BTX) quasi steady-state plumes were developed, two persulfate injection episodes were performed 10 d apart to create a chemical oxidation (ChemOx) zone. High-resolution monitoring was conducted to observe the migration of the ChemOx zone and transition into an EBR zone. Mass loss estimates and geochemical indicators were used to identify the distinct transition between the ChemOx and enhanced biological reactive zones. Compound specific isotope analysis (CSIA) was used to distinguish the dominant mass removal process, and to investigate the occurrence of microbial sulfate reduction. BTX metabolites and reverse-transcriptase quantitative polymerase chain reaction analyses of expressed biodegradation genes (as mRNA) were also used to characterize the response of indigenous microorganisms (especially sulfate-reducing bacteria) to the added persulfate. Multiple lines of evidence supported the conclusion that chemical oxidation was the dominant mass removal process in the vicinity of the injection zone, while enhanced biodegradation dominated BTX degradation in the downgradient portions of the system. The CSIA and supporting molecular biological data were critical in documenting temporally and spatially distinctive zones in this system that were dominated by either chemical-oxidation or anaerobic-biodegradation processes. Initially, persulfate had an inhibitory impact on the activity of the indigenous microbial community, but this was followed by a substantial rebound of microbial activity to above baseline levels. The results from this investigation demonstrate that the suite of diagnostic tools employed can be used to distinguish between chemical oxidation using persulfate and the subsequent effects of the produced sulfate.

Introduction

In situ chemical oxidation (ISCO) and enhanced bioremediation (EBR) are two technologies that have been extensively applied at sites contaminated with a variety of compounds including petroleum hydrocarbons (PHCs) (Sutton et al. 2010). ISCO involves the delivery of a strong oxidizing reagent into the subsurface to transform an organic contaminant into a less harmful intermediate or end-product such as CO_2 (Huling and Pivetz 2006). EBR involves the stimulation of indigenous hydrocarbon-utilizing microorganisms by delivering electron acceptors, electron donors (substrates), and/or nutrients to the subsurface (Reinhard et al. 1997; Bolliger et al. 1999; Cunningham et al. 2001; U.S. EPA 2013). Low cost, high efficiency, minimal impact on surface infrastructure, and adaptability to a variety of subsurface conditions and contaminant types are the potential advantages of these two technologies.

Despite its advantages, ISCO is inefficient in some situations due to geological heterogeneities, insufficient mixing, low oxidant persistence, and formation of troublesome by-products (e.g., MnO_2) (Lee and Kim 2002; MacKinnon and Thomson 2002; Xu and Thomson 2009). For example, oxidant delivery limitations have been shown to be responsible for a portion of the contaminant mass to persist following ISCO treatment, and the continuous slow mass transfer from this remaining residual mass leads to contaminant rebound and persistence of dilute plumes downgradient of source zones (Huling and Pivetz 2006; Thomson et al. 2008; Richardson et al. 2011; Sra et al. 2013a). In addition, ISCO is generally less cost-effective for the treatment of contaminants present at low concentrations. EBR is a less expensive technology for treating lower concentrations of

Article impact statement: Spatial and temporal mass removal in a persulfate/enhanced bioremediation (EBR) combined remedy successfully monitored with compound specific isotope analysis (CSIA) and molecular biological tools.

doi: 10.1111/gwmr.12227

contaminants; however, EBR is often only partially successful in degrading complex organic mixtures. Factors such as the availability of substrates, electron acceptors, and nutrients as well as the site-specific nature of the active microbial communities often limit the effectiveness of EBR (ITRC 2005). At many sites neither of these two technologies can be applied individually to achieve remediation objectives in a cost- and time-effective fashion (Devlin et al. 2004; Sahl and Munakata-Marr 2006; Sutton et al. 2010; Munakata-Marr et al. 2011).

Recent investigations have shown that the synergistic coupling or sequential use of ISCO and EBR could potentially combine the strengths of each individual technology and minimize their limitations (ITRC 2005). This technology integration approach (also referred to as a "combined remedy") has gained increased attention in recent years (Yang et al. 2005; Sahl et al. 2007; Tsitonaki et al. 2008; Sutton et al. 2010; Munakata-Marr et al. 2011). The general concept behind an integrated ISCO/EBR combined remedy is to use chemical oxidation to target the bulk of the contaminant mass in the zones with high concentrations, followed by the use of EBR to "polish" the remaining mass in the source zone and downgradient plume.

Among the widely used chemical oxidants, persulfate ($S_2O_8^{2-}$) has been used extensively for soil and groundwater treatment due to its capability to nonselectively destroy a wide range of environmentally relevant contaminants including PHC compounds (Huang et al. 2005; Liang et al. 2008; Sra et al. 2013a, 2013b). Unlike permanganate, persulfate is able to oxidize aromatic hydrocarbons and other fuel-related compounds without activation (Sra et al. 2013a, 2013b). Compared to peroxide and ozone, persulfate is more stable and can persist in the subsurface for weeks to months due to its low natural oxidant interaction (NOI) (Sra et al. 2010). These characteristics make persulfate an attractive choice for a chemical oxidant to treat PHC-impacted soils and groundwater. An additional advantage of using persulfate in a persulfate/EBR treatment system is the production of an excess amount of sulfate which results from persulfate decomposition (reaction with organic compounds and aquifer materials). This excess sulfate can serve as a terminal electron acceptor and enhance subsequent microbial sulfate reduction processes. Therefore, a persulfate/EBR combined remedy is expected to link the aggressive nature of persulfate oxidation to enhanced microbial sulfate reduction.

Microbial sulfate reduction is mediated by a diverse group of microorganisms known as dissimilatory sulfate reducing bacteria (SRB) which are abundant in anoxic environments, such as PHC-contaminated aquifers. SRB communities capable of complete oxidation of benzene, toluene, and *o*-xylene (BTX) have been previously identified (Beller et al. 1996; Harms et al. 1999; Kleikemper et al. 2002; Miao et al. 2012). In general, the rate of microbial sulfate reduction is a function of the SRB specific growth rate, which in turn is controlled by the availability of sulfate and the organic substrate used by the microorganisms during energy production. The microbial sulfate reduction rate is expected to increase following the application of persulfate, due to (1) the breakdown of complex PHC compounds into simpler organic substrates that are more bioavailable (i.e., easily taken up and metabolized by a SRB cell), and (2) the production of additional sulfate which serves as the electron acceptor which is required for microbial maintenance and growth.

To design an effective integrated persulfate/EBR treatment system, it is necessary to understand the interactions between persulfate and the indigenous microbial communities. The impact of chemical oxidants on biological processes has been previously reviewed and summarized by others (e.g., Sahl and Munakata-Marr 2006). These studies have predominantly focused on the impact of conventional oxidants (i.e., hydrogen peroxide, ozone, and permanganate) on aerobic microorganisms indigenous in aquifers contaminated with polyaromatic hydrocarbons or chlorinated solvents. The general observations from these studies have been an increase in microbial populations and stimulation of biodegradation activity following the application of an oxidant which led to enhanced removal of contaminant mass. In some cases, an initial inhibition of the microbial activity was observed in the presence of higher oxidant concentrations; however, a rebound of the microbial population and activity was reported within a few days to months following oxidant application.

There exist only a few peer-reviewed studies that have investigated in the laboratory the impact of persulfate on the abundance and activity of indigenous microorganisms. In a series of batch experiments, Tsitonaki et al. (2008) exposed aquifer material contaminated with landfill leachate to various doses of heat-activated persulfate (0.02 to 2 g/kg) and monitored both the change in cell density and conversion of acetate to carbon dioxide by the indigenous aerobic communities, with and without addition of a laboratory strain, *Pseudomonas putida* KT2440. In these microcosms, Tsitonaki et al. (2008) found that persulfate concentrations up to 10 g/L had no adverse impact on the native microbial community, and that persulfate was less inhibitory to indigenous microorganisms than other oxidants tested (iron catalyzed hydrogen peroxide, and permanganate). The same observation was reported by Cassidy et al. (2009) who compared the effect of ozone, modified Fenton's reagent, and iron-activated persulfate on subsequent aerobic biodegradation of 2,4-dinitrotoluene in batch slurry reactors. Richardson et al. (2011) investigated the impact of persulfate on the abundance and activity of the indigenous microbial community and on phenanthrene-degrading bacteria present in contaminated soil from a former manufactured gas plant site. Following the injection of 20 g/L persulfate in a column experiment, Richardson et al. (2011) used 16 rRNA gene assays to characterize the microbial community and also measured the conversion of ^{14}C-labeled substrates to $^{14}CO_2$ by the microbial community. This study showed that exposure to persulfate initially led to inhibition of microbial activity, a decrease in community diversity, and to reductions in the abundances of both total and phenanthrene-degrading populations; however, recovery was observed within 14 to 70 weeks.

In the gray literature, the impact of persulfate on the composition and diversity of SRB communities has been documented in several laboratory experiments (Bou-Nasr et al. 2006; Gallagher and Crimi 2007; Cassidy 2008) and observed at field sites contaminated with chlorinated hydrocarbons (Droste et al. 2002; Marley et al. 2006; Sessa

et al. 2008; Studer et al. 2009). Unfortunately none of these studies are representative of an engineered persulfate/EBR combined remedy and, at best, provide information on the temporal but not the spatial separation of chemical and biological treatment zones. Moreover, prior studies have not provided detailed characterization of the processes involved in a persulfate/EBR combined remedy. Also, no previous effort has investigated the impact of persulfate on subsequent microbial degradation processes in a field system. Thus, to improve our understanding of the treatment of a groundwater system impacted with PHCs using persulfate coupled with sulfate reducing biodegradation, a pilot-scale experiment was designed and executed. A unique design approach was used to enclose a portion of a dissolved phase PHC plume between two persulfate injection pulses. This enclosed segment of the plume was then monitored as the chemical oxidation zone transitioned into an enhanced-bioremediation zone downgradient.

The main objectives of this field effort were to characterize the processes involved in a combined persulfate/EBR remedy, to identify the temporal and spatial boundaries and transitional points between the various processes, and to assess the impact of persulfate on microbial processes (especially, biodegradation under sulfate reducing conditions). To achieve these objectives, conventional groundwater parameters were augmented with isotopic and molecular-biological procedures.

Methods

General

Figure 1 illustrates the conceptual approach adopted for this pilot-scale trial. Initially, a dissolved (quasi steady-state) plume of BTX compounds was generated using a diffusive source to develop an anaerobic aquifer system, and to provide favorable conditions for the acclimation and growth of indigenous SRB (Figure 1a). Next, two sequential persulfate injection episodes were executed to treat a portion of the dissolved phase plume (Figure 1b and 1c). Due to longitudinal dispersion, the two persulfate slugs were expected to mix with the confined portion of the BTX plumes as they migrated downgradient (Figure 1d) to form a chemical oxidation (ChemOx) zone. As the BTX and persulfate mass was depleted due to chemical oxidation, a sulfate plume was expected to form and the ChemOx zone was expected to transition into an EBR zone. It was postulated that the migration of the sulfate plume would stimulate the growth and activity of the indigenous SRB within the EBR zone (Figure 1e). BTX mass removal in the ChemOx zone was expected to be dominated by chemical oxidation, and in the EBR zone by enhanced microbial sulfate reduction. Note that the diffusive PHC source used here to establish a dissolved BTX plume does not reflect the complexity of an actual nonaqueous phase liquid source zone. To monitor the fate of the ChemOx and EBR zones, and to detect the biogeochemical shifts prior to, during, and following persulfate injection, a host of groundwater parameters were monitored. These included geochemical indicators (dissolved oxygen [DO], electrical conductivity [EC], redox potential [Eh], and pH), dissolved inorganic carbon (DIC) content, and the concentration of BTX, methane, and selected inorganic species (e.g., persulfate, SO_4^{2-}, Na^+, Ca^{2+}, S^{2-}). However, evaluating the impact of persulfate oxidation on the subsequent microbial processes only through concentration patterns of SO_4^{2-}, S^{2-} and/or changes of DIC content is likely a challenge at most sites due to the system dynamics and the potential dilution, dispersion, sorption, and abiotic processes (e.g., mineral precipitation). Thus to aid in this characterization effort, compound specific isotope analysis (CSIA) and biomarkers (GC/MS analysis of metabolites and quantitative polymerase chain reaction (qPCR) methods of expressed biodegradation genes) were utilized.

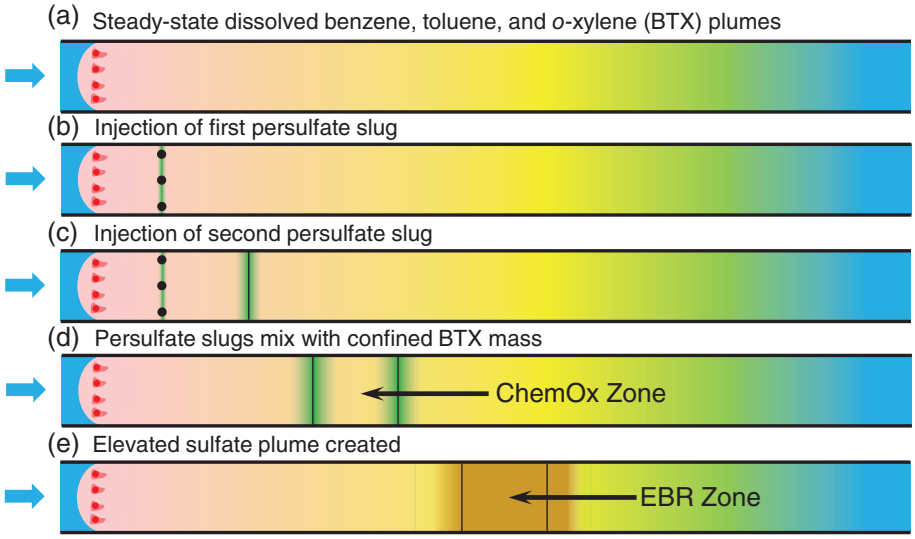

Figure 1. Conceptual representation of the pilot-scale experiment: (a) the generated quasi steady-state BTX plumes, (b) first persulfate injection downgradient of the dissolved plume source, (c) second persulfate injection, (d) formation of the ChemOx zone between the two persulfate slugs where mixing and the reaction between persulfate and the dissolved BTX mass occurs, and (e) depletion of ChemOx zone due to persulfate decomposition and generation of a sulfate plume (EBR zone) where enhanced microbial sulfate reduction is expected to occur.

Specific chemical and biological mass removal processes (e.g., aerobic/anaerobic biodegradation, or chemical oxidation) have been shown to exhibit distinctive carbon and hydrogen (C/H) isotopic fractionation patterns that have been documented for many organic contaminants (Morasch et al. 2001; Poulson and Naraoka 2002; Hunkeler et al. 2003; Mancini et al. 2003; Marchesi et al. 2013). In this study, dual carbon and hydrogen CSIA ($\delta^{13}C$ and $\delta^{2}H$) was used to characterize the fate of the BTX compounds and to identify the dominant mass removal process. For this purpose, the isotope data for BTX compounds were compared to the dual element isotope slopes reported in the literature for biodegradation and persulfate oxidation of these compounds. In addition, to investigate the occurrence and extent of the subsequent microbial sulfate reduction process, temporal patterns of oxygen and sulfur isotopes ($\delta^{18}O$ and $\delta^{34}S$) in SO_4^{2-} were also tracked.

For diagnostic purposes, the most informative biomarker metabolites are those whose molecular structure strongly resembles that of the parent contaminant; these occur early in the metabolic pathways (Table S1a, Supporting Information). In this study, we analyzed a total of 12 metabolites (Table S1a). Four of these metabolites are uniquely of microbial origin (benzene *cis*-dihydrodiol, indicative of aerobic benzene degradation (Diaz et al. 2013; Cébron et al. 2008; Gülensoy and Alvarez 1999; Nebe et al. 2009; Wilson and Madsen 1996); toluene *cis*-dihydrodiol, indicative of aerobic toluene degradation (Diaz et al. 2013; Cébron et al. 2008; Gülensoy and Alvarez 1999; Nebe et al. 2009; Wilson and Madsen 1996); benzylsuccinate, indicative of anaerobic toluene degradation (Beller et al. 2008; Fuchs et al. 2011); and 2-methylbenzylsuccinate, indicative of anaerobic xylene degradation (Beller et al. 2008; Fuchs et al. 2011). Other metabolites detected in groundwater samples include *o*-cresol (strongly associated with aerobic xylene biodegradation), 2,3-dimethylphenol (strongly associated with aerobic xylene biodegradation), phenol (strongly associated with both aerobic and anaerobic benzene biodegradation), and benzoate (strongly associated with both aerobic toluene biodegradation and anaerobic benzene degradation) (Whited and Gibson 1991; Diaz et al. 2013; Hendrickx et al. 2006).

A parallel strategy for documenting biodegradation as an active process utilizes the biomarker known as "mRNA" (messenger RNA, Table S1b). Documenting the occurrence of mRNA of biodegradation genes in groundwater shows that microorganisms hosting the DNA that encodes biodegradation enzymes are metabolically active and engaged in the biodegradation process. Assays detecting mRNA of the *todC* (aromatic dioxygenase) and TOL (side-chain monooxygenase) genes can be positive during the biodegradation of BT under aerobic conditions (Cébron et al. 2008; Hendrickx et al. 2006; Nebe et al. 2009); only data from *todC*-based assays are reported in the present investigation because TOL assays were negative when tested. To date the genetic basis for only a single metabolic pathway for anaerobic benzene biodegradation has been reported: the *abcA* gene (anaerobic benzene carboxylase) is characteristic of benzene biodegradation under iron-reducing and other anaerobic conditions (Abu Laban et al. 2010). The *bssA* gene (and corresponding mRNA) encodes biodegradation of TX under anaerobic conditions (Fuchs et al. 2011, Kazy et al. 2010) and a specific variant of the *bssA* gene, *bssA-SRB,* has been shown to be carried by bacteria that are active in anaerobic toluene metabolism under sulfate-reducing conditions (Beller et al. 2008). Thus, detecting mRNA of the *bssA*-SRB gene links biodegradation of toluene to populations carrying out sulfate reduction. In addition, respiratory reduction of sulfate in anaerobic habitats has been mechanistically linked to the expression of the alpha and beta subunits of the dissimilatory (bi)sulfite reductase genes, *dsrA* and *dsrB*, respectively (Bourne et al. 2011, Geets et al. 2006; Chin et al. 2008; Neretin et al. 2003; Pelikan et al. 2016).

Site Description

This pilot-scale experiment was conducted in a sheet pile-walled gate at the University of Waterloo Groundwater Research Facility at the Canadian Forces Base (CFB) Borden located near Alliston, ON. As shown in Figure 2 and Figure S1a, the experimental gate used was 2 m wide and 24 m long, and was enclosed on three sides by sheet piling driven 3 m below ground surface (bgs) into the underlying aquitard. The fourth side was open to allow ambient

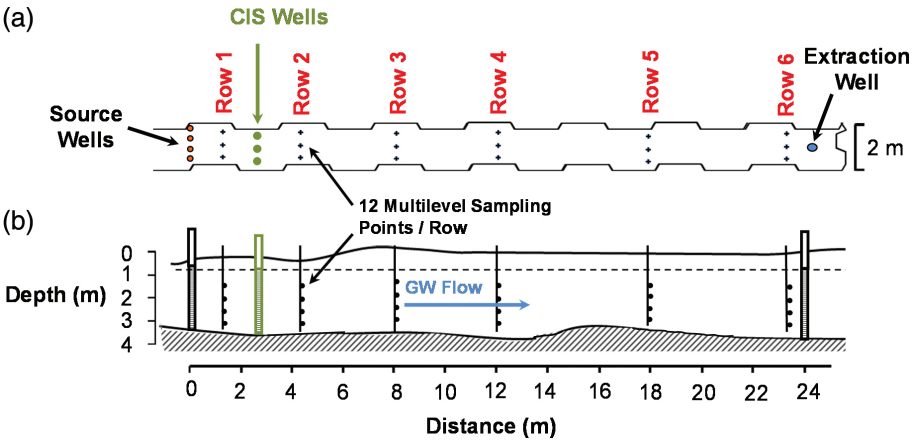

Figure 2. (a) Plan view, and (b) cross-sectional view of the experimental gate. The cross-injection system (CIS) wells used to delivery persulfate into the gate upgradient of Row 2 are indicated.

groundwater to enter. Four source wells installed at the gate entrance (fully screened, 25.4 cm diameter) were used to introduce the source of BTX into the system. A pump was installed in the well at the downgradient closed end of the gate (fully screened, 5.1 cm diameter) to control the groundwater flow rate.

The monitoring network consisted of six fence lines at various locations along the length of the gate (identified as Row 1 to Row 6). Each row consisted of three multilevel (ML) monitoring wells (identified as left, middle, and right in the direction of groundwater flow). The wells in each row were spaced 0.65 m apart and each was equipped with four multilevel sampling points spaced vertically at an interval of 0.7 m with the shallowest multilevel starting at 1.2 m bgs. For persulfate delivery, three wells (fully screened below the water table, internal diameter of 5.1 cm) were installed between Row 1 and Row 2 (Figure 2 and Figure S1c).

The unconfined Borden aquifer is a surficial, well-sorted fine to medium-grained sandy aquifer with a hydraulic conductivity of 6.0×10^{-6} to 2.0×10^{-4} m/s. Microscale heterogeneities exist in the form of silty sand and coarse sand lenses (Mackay et al. 1986). General hydrogeological properties and background geochemistry of the Borden aquifer have been extensively characterized (e.g., MacFarlane et al. 1983; Nicholson et al. 1983; Mackay et al. 1986). The natural organic matter (NOM) content or fraction of organic carbon (f_{oc}) of the aquifer material is 0.0002, and the aquifer porosity is approximately 0.33. The background concentration of SO_4^{2-}, Na^+, Ca^{2+}, and H_2S varies from 10 to 30 mg/L, 1 to 2 mg/L, 50 to 110 mg/L, and <0.002 to 0.1 mg/L, respectively. The groundwater pH is between 7 and 8.

Experimental Phases

Plume Generation (Phase 1)

To facilitate the controlled release of the selected BTX compounds at the gate entrance, a series of Waterloo Emitters (Model 703, Solinst Canada Ltd., Georgetown, Ontario, Canada) were placed into the source wells (Figure S1b). Each emitter device consisted of 46 m of low-density polyethylene (LDPE) tubing (6.4 mm in diameter) coiled around a central PVC frame (130 cm in length, 15 cm in diameter). The mass transfer from an emitter is controlled by molecular diffusion (driven by the concentration gradient between the source solution circulating inside the emitter tubing and the by-passing ambient water) and advection (driven by the flow rate of the by-passing water) (Arildskov and Devlin 2000; Wilson and Mackay 1995a, 1995b). The purpose of the passive emitters was to maintain a continuous transfer of BTX compounds from the source solution into the groundwater passing through the wells.

Within the experiment gate, eight Waterloo Emitters were placed inside the four source wells (two emitters per well stacked on top of each other) to create a semi-uniform steady source of dissolved BTX compounds. To circulate the source solution through the emitters, the emitters in each source well were connected using a 3.2 mm diameter stainless steel tube to one source tank (total four source tanks). The source solution was pumped at a rate of approximately 50 mL/min through the emitters on a timed cycle of 6 h circulation followed by 6 h off. Each source tank contained 90 L of water and 10 L of ethanol spiked with the BTX mixture. The initial average concentration of BTX in the four source tanks was 380, 320, and 70 mg/L, respectively (Figure S3). A series of laboratory experiments showed that that the ability of ethanol to diffuse out of the emitters was insignificant compared to toluene. The source tanks were sealed to avoid volatilization, and the stock solution was stirred periodically with a drill-adapted mixing rod. As the stock solution was circulated, the BTX concentration in the source tanks would deplete over time due to the loss of BTX mass into the source wells. To maintain the BTX concentration at a quasi-constant level in the source wells, the tanks were occasionally replenished (approximately every 50 d) by removing 10 L of the source tank solution and adding 10 L of the ethanol/BTX mixture to each tank.

The groundwater flow rate was controlled by the extraction well located at the closed end of the experimental gate. To estimate the groundwater velocity, a tracer test was conducted by injecting a slug of a sodium chloride (NaCl) solution directly into the four source wells to reach a target chloride (Cl^-) concentration of 100 mg/L. The transport of chloride was monitored downgradient of the source wells, and the resulting breakthrough data were used to estimate velocity.

Chemical Oxidation (Phase 2)

Phase 2 of the experiment involved two injections of persulfate into the BTX plume using a modified cross-injection system (CIS) (Devlin and Barker 1996; Gierczak et al. 2007) installed between Row 1 and Row 2 (Figure 2a and Figure S1c). The persulfate solution was injected into the two outside CIS wells (0.5 L/min each) while groundwater was simultaneously extracted from the central CIS well (1.0 L/min) and transferred to a polyethylene (PE) waste tank. Each injection episode was used to create a persulfate slug a short distance downgradient of the CIS wells. The extent of the ChemOx zone, confined between the two persulfate pulses, depends on the groundwater flow rate. An interval of 10 d between each injection episode was selected so that the fate of the ChemOx zone (e.g., depletion of persulfate and BTX, production of sulfate, and geochemical shifts) could be captured in the first monitoring row downgradient of the CIS wells (i.e., Row 2).

An intended outcome of Phase 2 was to partially destroy the BTX mass in the ChemOx zone, so that the remaining substrate would serve as the carbon/energy source for the subsequent microbial activity. To estimate the amount of persulfate required to destroy approximately 50% of the mass confined in the ChemOx zone, the BTX mass in this zone was estimated from the BTX mass discharge across Row 1 and using reaction stoichiometry between unactivated persulfate and the individual organic compounds (Sra et al. 2013b). Sra et al. (2013b) also provide useful data on first-order oxidation rate coefficients for BTX compounds degraded by unactivated or activated persulfate.

The injection solution (10 g/L unactivated sodium persulfate [$Na_2S_2O_8$]) was prepared by mixing sodium persulfate (Sigma-Aldrich, St. Louis, Missouri) with uncontaminated groundwater. The solution was stored in a PE tank and was mechanically stirred using an electric drill mixer to enhance dissolution. A manifold was used to distribute the injection

solution into two Teflon tubes connected to the injection wells. Each of these outlets was equipped with a flow control gate valve, a vent valve and a pressure gauge to enable flow control during injection. PE pipes were used to connect the manifold outlets to the riser pipes of the three CIS wells.

Extended Monitoring (Phase 3)

An assessment of the treatment system was continued for several months following persulfate injection to monitor the fate of the ChemOx and EBR zones, to evaluate the long-term impact of persulfate on the subsequent microbial processes, and to identify the dominant mass removal process.

Sampling and Analytical Methods

Groundwater samples were collected at multilevel locations using a peristaltic pump and a sampling manifold (Mackay et al. 1986). Prior to collecting samples, each sampling point was purged approximately 80 mL to flush the water inside the tubing and the sampling manifold to ensure the collected samples were representative of the groundwater adjacent to the sampling point. Samples for persulfate analysis were collected in 25 mL glass vials, and samples for inorganic analyses were collected in 20 mL polypropylene vials. Samples collected for cation analyses were filtered with a 0.45 µm syringe membrane filter, and acidified with nitric acid (Sigma-Aldrich, St. Louis, Missouri) to a pH < 2. Samples for VOC analysis and samples for C/H isotopic analyses were collected in 40 mL glass vials and preserved with 0.4 mL of a 10% sodium azide solution. Samples for isotope analysis of sulfate were collected in 1 L glass bottles without addition of preservatives. Samples for analysis of metabolites were collected in two 500 mL glass bottles at each sampling point. The metabolite samples were immediately preserved by adding HCl (J.T. Baker, Phillipsbourg, New Jersey) to one of the bottles with a target pH of <2, and NaOH (Fisher Scientific, Fair Lawns, New Jersey) to the other bottle with a target pH of approximately 8. All samples were stored at 4 °C and held for up to 14 d prior to analyses. The samples for qPCR analyses were collected by passing 2 L of groundwater through a 0.2 µm Sterivex filter (Millipore, Billerica, Massachusetts). The filter was then frozen immediately, and stored at −80 °C until further processing. While there is no doubt that some perturbation to the system resulted from sampling, we believe this did not significantly affect the results (total sampling volume 5.8 L, groundwater discharge between sampling intervals ~7000 L). Details of the analytical methods used to: (1) quantify the concentration of organic compounds and inorganic species; (2) analyze the carbon ($^{13}C/^{12}C$), hydrogen ($^{2}H/^{1}H$): sulfur ($^{34}S/^{32}S$), and oxygen ($^{18}O/^{16}O$) isotope ratios; (3) extract and analyze DNA and RNA from groundwater biomass; and (4) identify specific metabolites are provided in the Appendix S1.

Results and Discussion

The generation of the BTX plumes began on Day 0 by turning on the extraction pump and allowing the transport of BTX compounds from the source tanks to flow into the emitters installed in the source wells. The two persulfate pulsing episodes were conducted on Day 170 and Day 180. Due to the onset of winter conditions, the system was shutdown on Day 221 by turning off the extraction pump and flow to the emitters. Extended monitoring was continued until Day 391. Figure S2 shows a detailed timeline including the timing of the various groundwater sampling events.

Phase 1—Plume Generation (Day 0 to Day 169)

On Day 0, the groundwater extraction rate was set to 125 mL/min to establish a theoretical groundwater Darcy velocity of 9 cm/d (equal to the ambient groundwater velocity in the Borden aquifer) based on the extraction rate and aquifer properties (e.g., porosity and aquifer thickness). The conservative tracer test which was performed by adding NaCl into the source wells over a 2-week period (Days 5, 14, and 20) created a slug of tracer downgradient. Chloride concentrations were monitored at 12 points in Row 1, and the groundwater velocity was calculated based on the observed travel time of the center of mass of the chloride breakthrough curve and distance between the source wells and Row 1. The estimated groundwater velocity from the observed tracer data ranged from 7 to 12 cm/d across the 12 monitoring points (Figure S3). Since the theoretical Darcy velocity approach was consistent with the estimate from the tracer test data, it was used during the course of this experiment to estimate the average groundwater velocity in the gate. The average concentration of BTX in all four source wells during the plume generation phase was approximately 55, 40, and 10 mg/L, respectively. Figure S3 shows the temporal variation of the average BTX (sum of BTX) concentration from Day 0 to Day 221 in the four source tanks and four source wells.

The development of the BTX plumes until Day 156 (before persulfate injection) is shown in Figure 3. The nonuniform distribution of BTX concentrations across the gate cross-section, which was also observed for the chloride plume (data not shown here), indicates the existence of preferential flow pathways which result from the mildly heterogeneous nature of the aquifer. By Day 97 the front of the benzene plume had reached only 2 of the 12 multilevel sampling points in Row 3 (located only 7.5 m downgradient of the source wells), while based on the average groundwater velocity the advective front was expected to be approximately 9 m from source wells (past Row 3). The delay in plume development between Day 35 and Day 97 as a result of sorption and biodegradation was indicated by: (1) decreased BTX concentrations at Row 1 (between Day 35 and Day 71) while the source well concentrations were continually increasing (data not provided); (2) decreased BTX concentrations at Row 2 (between Day 71 and Day 97) while the mass discharge from Row 1 was stable; and (3) minimal benzene mass, and no toluene and *o*-xylene mass detected at Row 3 located 7.5 m downgradient of the source wells (Figure 4). Biodegradation in the vicinity of Row 1 and Row 2 was confirmed by decreased DO and Eh levels (Figure 5a and 5c), and supported by the detection of biomarkers (metabolites and mRNA copies) characteristic of both aerobic and anaerobic BTX biodegradation (Figure 6).

Since the intended result from the plume generation phase was to develop a quasi steady-state BTX plume and establish anaerobic conditions throughout the experimental gate, the

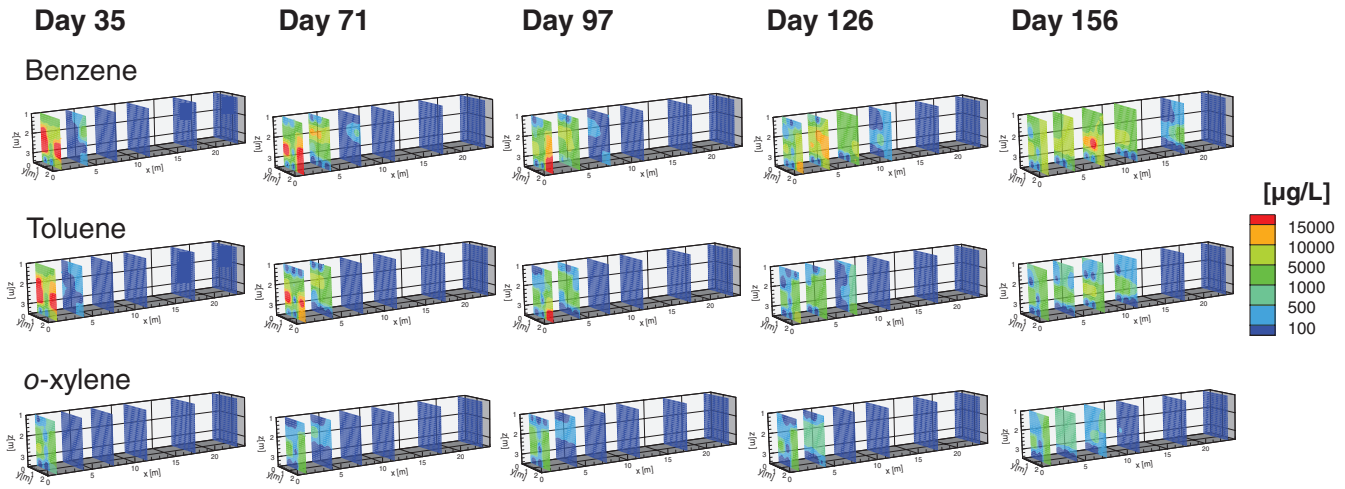

Figure 3. Development of the benzene, toluene, and *o*-xylene plumes during the plume generation phase (Phase 1). All three plumes followed the same general pattern. The slower migration of toluene and xylene plumes compared to benzene plume is attributed to a higher sorption capacity and biodegradation rate. Between Day 72 and Day 97 the expansion of the plumes appeared to stop as a result of natural attenuation processes, and hence the groundwater velocity was increased on Day 110 to encourage the plumes to migrate further downgradient as seen on Day 156.

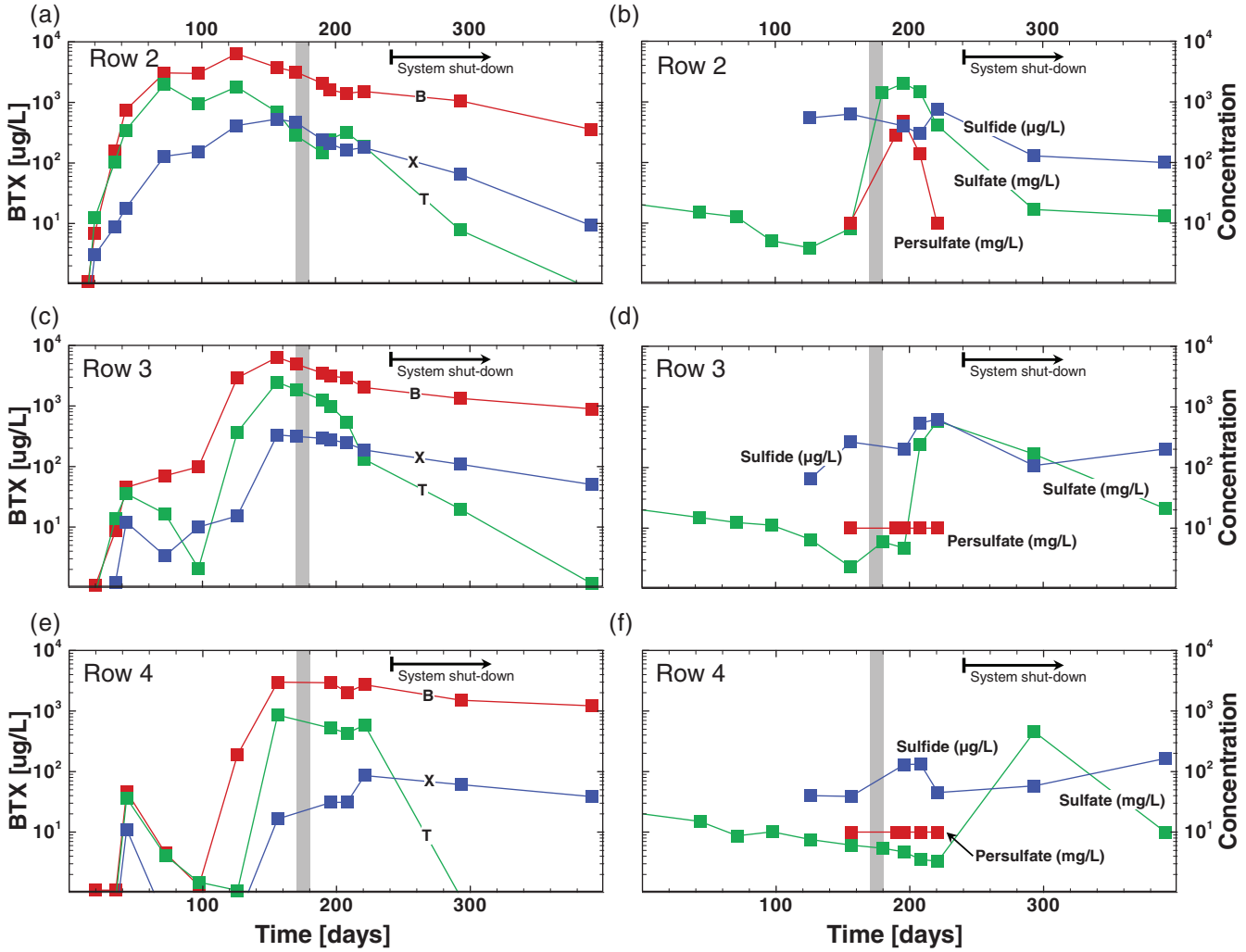

Figure 4. Row-averaged (based on weighted cross-sectional area) BTX (µg/L), persulfate (mg/L), sulfate (mg/L), and sulfide (µg/L) breakthrough curves at (a and b) Row 2, (c and d) Row 3, and (e and f) Row 4. The gray band between Day 170 and Day 180 indicates the chemical oxidation phase (Phase 2).

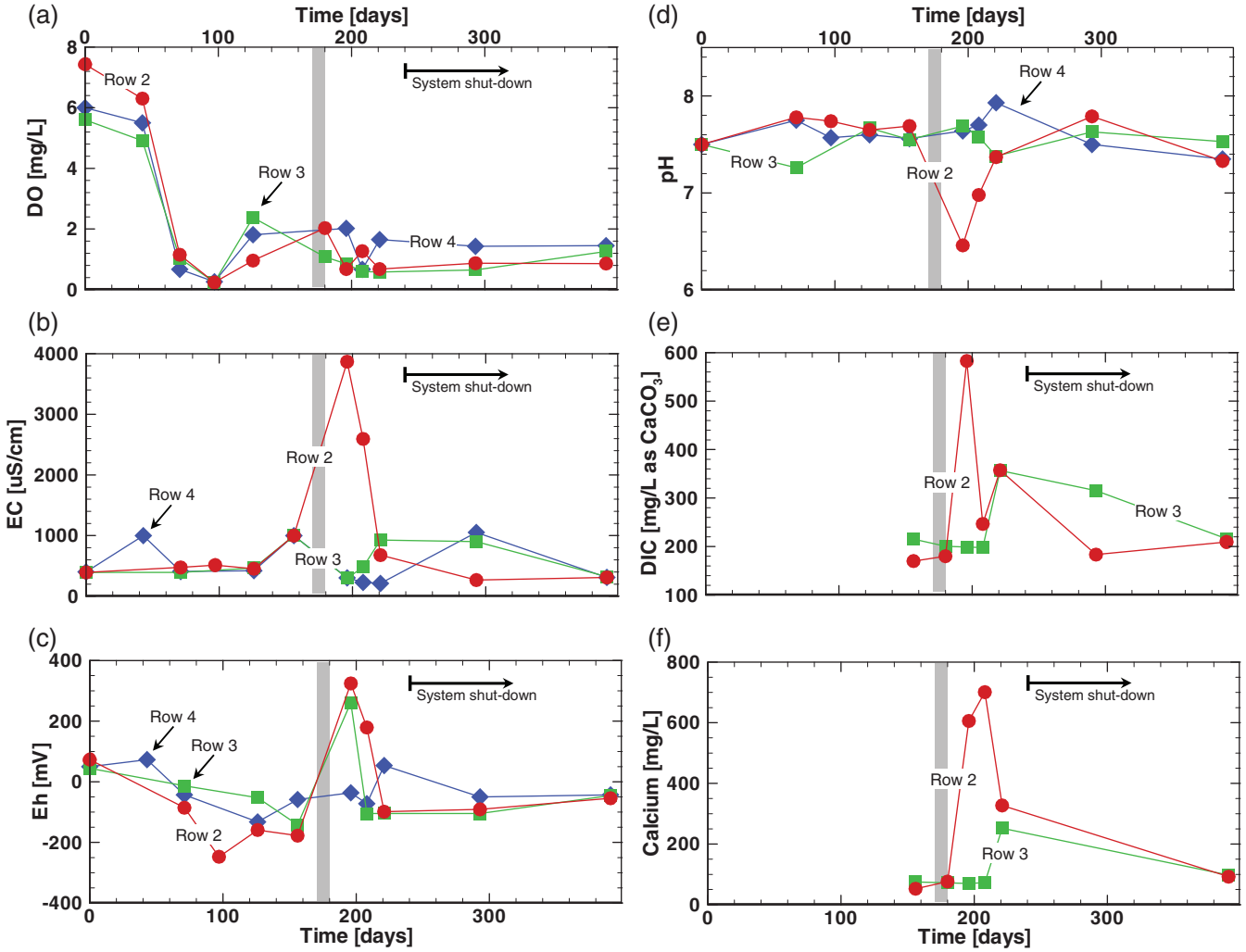

Figure 5. Temporal evolution of geochemical indicators (row-averaged based on weighted cross-sectional area): (a) dissolved oxygen, (b) electrical conductivity, (c) oxidation–reduction potential (Eh), (d) pH, (e) dissolved inorganic carbon (DIC) content in mg/L as $CaCO_3$, and (f) calcium concentration. The gray band between Day 170 and Day 180 indicates the chemical oxidation phase (Phase 2).

groundwater extraction rate was increased to 425 mL/min on Day 110 to counterbalance the impact of biodegradation processes on plume development. As a result, the migration of the plume was significantly enhanced, and by Day 126 the benzene plume was detected at a significant number of multilevel sampling points in Row 4 (Figures 3 and 4). On Day 140, the extraction rate was reduced to approximately 150 mL/min (15 cm/d) and held constant until Day 221. By Day 156 (the last sampling event before persulfate injection) the benzene plume had reached Row 5 (Figure 3), DO was depleted (DO <2 mg/L) and reducing redox conditions prevailed throughout the entire the experimental gate (−200 mV < Eh < −50 mV) (Figure 5c). The increased BTX concentrations at Row 4 on Day 156 (Figure 4e) is attributed to the increased mass discharge from the upgradient rows following the increase in extraction rate; however, a decrease in BTX concentration was observed at Rows 1, and 2 after Day 110 (data not provided). This decrease is attributed to the mixed effect of decreased groundwater residence time in the source wells, and increased microbial activity. The lack of a uniform extraction rate for the entire experimental period was implemented out of necessity knowing full well that it would confound data interpretation but not harm the overarching objectives of this investigation.

Figure 6 shows the evolution of biomarkers observed at Rows 1, 2, and 3 that are unique to aerobic biodegradation of aromatics (*todC* mRNA and *cis*-dihydrodiols) (Figure 6a to 6c), that are unique to anaerobic biodegradation of aromatics or sulfate reduction (*bssA* and *bssA-SRB* mRNA and benzylsuccinates) (Figure 6d to 6f), and other metabolites characteristic of aerobic aromatic metabolism (*o*-cresol, 2,3 DMP) or that can be produced both aerobically and anaerobically (phenol, benzoate) (Figure 6g to 6i). Cresols are metabolites representing monooxygenase attack of toluene; unexpectedly, assays aimed at detecting mRNA from expressed TOL monooxygenase genes (Hendrickx et al. 2006) were not successful. Because the maximum absolute number of mRNA copies in Figure 6d to 6f ranged from 150 to 1.1×10^7/L the ordinate values for the mRNA series are plotted on a log scale. Likewise, the maximum absolute concentrations for metabolites shown in Figure 6g to 6i ranged from 5 to 390 µg/L; thus, these values are also plotted on a log scale. A key feature of patterns revealed by the biomarker analyses is that major aerobic metabolites

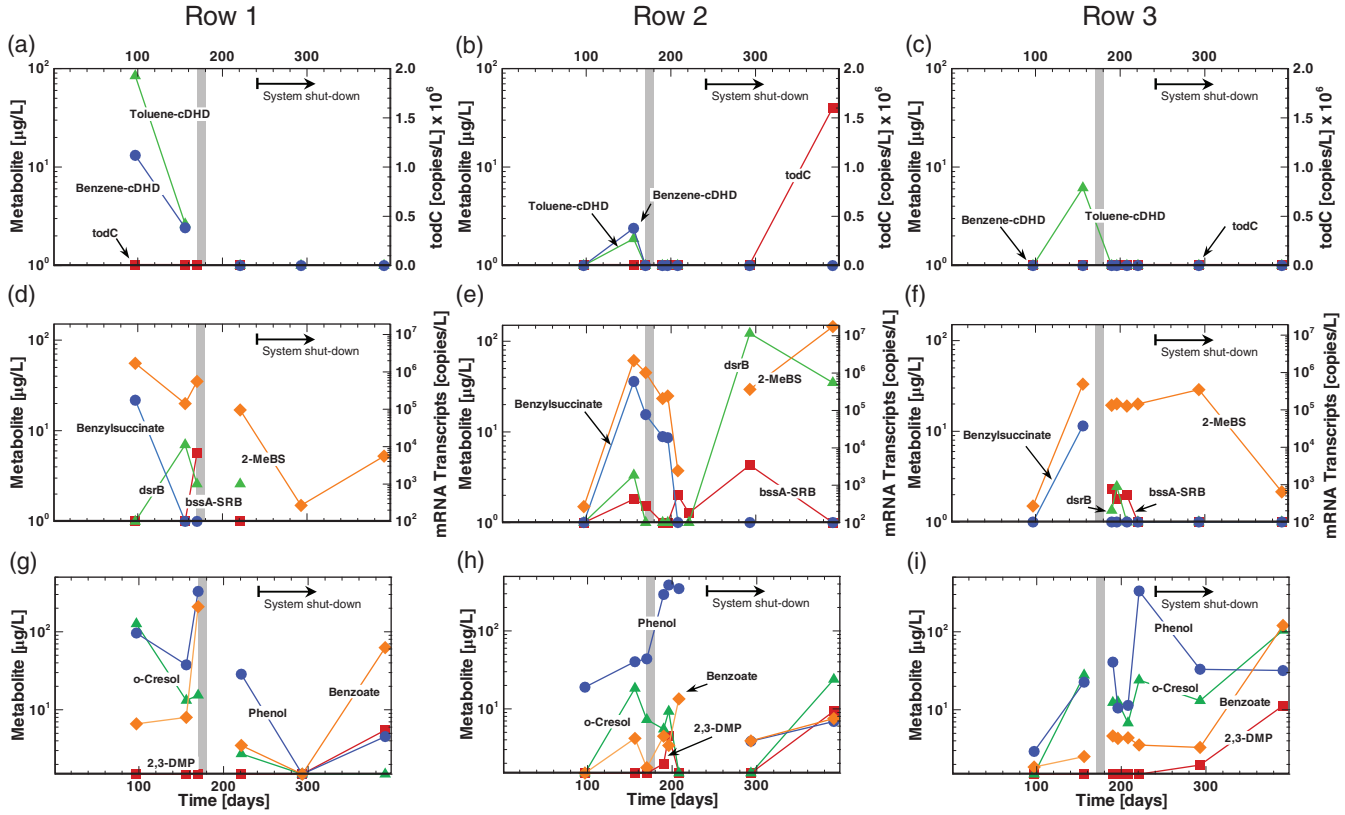

Figure 6. Temporal patterns in the appearance of biomarkers (mRNA and metabolites) at approximately 2.6 m bgs at Row 1 (left ML), Row 2 (left ML), and Row 3 (middle ML). Panels (a to c) show biomarkers (todC [toluene dioxygenase] mRNA and cDHDs [*cis*-dihydrodiols]) unique to aerobic biodegradation of aromatics. Panels (d to f) show biomarkers (bssA-SRB [benzylsuccinate synthase] mRNA and dsrB [dissimilatory sulfate reductase] mRNA, and benzylsuccinate, and 2-MeBS [2-methyl benzylsuccinate]) unique to anaerobic biodegradation of aromatics or sulfate reduction. Panels (g to i) show other metabolites characteristic of aerobic aromatic metabolism (*o*-cresol, 2,3-dimethylphenol [DMP]) or that can be produced both aerobically and anaerobically (phenol, benzoate). The gray band between Day 170 and Day 180 indicates the chemical oxidation phase (Phase 2).

(benzene- and toluene-cis dihydrodiol [CDH] and *o*-cresol) were found at maximum concentrations at Row 1 at early times (Figure 6a and 6g), before drastically declining; these compounds were also found in Row 2 and 3 on Day 156, but at concentrations far lower than at Row 1. These data support the notion that aerobic biodegradation contributed significantly to initial BTX removal. Anaerobic metabolites characteristic of both toluene and xylene biodegradation (benzylsuccinate, 2-methylbenzyl succinate, respectively) were also detected in all three rows (Figure 6d to f, Table S3), showing that the native microbial community was engaged in anaerobic TX degradation. The co-occurrence of both aerobic and anaerobic processes is a result of sampling groundwater for microbial analyses from adjacent aerobic and anaerobic microsites. Interestingly, evidence for relatively high general microbial activity was uncovered by measuring the concentrations of both phenol and benzoate (of possible aerobic and anaerobic origin), which peaked on Day 170 at Row 1 (Figure 6g).

mRNA transcripts characteristic of sulfate-based biodegradation of toluene and xylene (*bssA*-SRB) were found in Rows 1 and 2 on Days 156 and/or Day 170 in quantities ranging from 3×10^2 to 7×10^3 copies /L; Figure 6d and 6e). Also, *dsrB* mRNA transcripts (characteristic of sulfate reduction) were found on Day 156 in Rows 1 and 2 at levels ranging from 1×10^4 to 2×10^2 copies/L, respectively (Figure 6d and 6e; Table S3). These mRNA data provide evidence that the native microbial populations were engaged in sulfate-based biodegradation of methylated aromatics (e.g., toluene and xylene) and in sulfate reduction, respectively. Concurrent geochemical measurements independently showed that, by Day 156, sulfate-reducing conditions were present in the vicinity of Rows 2 and 3, as indicated by the simultaneous depletion of the background SO_4^{2-} and the production of S^{2-} (Figure 4b and 4d). On no occasion in this investigation were transcripts for anaerobic benzene degradation (*abcA*) detected.

Taken together, the data on plume migration, geochemistry, and biomarkers (Figures 3 through 6) document that natural attenuation of BTX became established during Phase 1 and that initial aerobic biodegradation was followed by sulfate-reduction-based metabolism consistent with findings reported by others (e.g., Acton and Barker 1992). These observations confirm the development of quasi steady-state BTX plumes, the establishment of anaerobic conditions, and manifestation of mass removal due to biodegradation processes along the experimental gate prior to first persulfate injection on Day 170. The benzene plume had migrated beyond Row 5 (~18 m downgradient) while the toluene and xylene plumes were retarded due to their higher sorption capacity and biodegradability relative to benzene (Schirmer et al. 2000).

Phase 2—Chemical Oxidation (Day 170 to Day 180)

The first persulfate injection episode was conducted on Day 170. During this 3 h episode, groundwater samples were collected and EC measurements were taken every 20 min. The persulfate concentration in the injection wells was much higher than that in the central extraction well (13 vs. 1 g/L). To create a more uniform persulfate slug across the gate, the duration of the second episode (executed on Day 180) was increased to 5 h, and the injected target persulfate concentration was increased from 10 to 15 g/L. This increased duration and concentration resulted in a persulfate concentration of approximately 4 g/L in the extraction well compared to a persulfate concentration of 16 g/L in the two injection wells. Based on these data, neither of these two injection episodes was able to create a uniform persulfate slug. The 10-d interval between the two injection episodes was to ensure that the ChemOx zone was of sufficient length by the time it reached Row 2. This interval was based on the estimated groundwater velocity at the time of the persulfate injections (15 cm/d), the distance between the CIS wells and Row 2 (1.5 m), and assuming negligible retardation for persulfate and sulfate.

As a result of the two injection episodes, a total of approximately 4.7 kg of persulfate was estimated to have been present initially in the gate. The increased EC and Eh levels at Row 2 following persulfate injection (Figure 5b and 5c) as well as the observed breakthrough of persulfate and Na^+ (Figure S4) demonstrates the length of the ChemOx zone as it passed across Row 2. Only one persulfate peak (on Day 196) and one Na^+ peak (on Day 208) was observed at Row 2 suggesting that the two persulfate slugs had coalesced before reaching Row 2 as designed; however, the sampling resolution may have missed two peaks. The retardation of Na^+ compared to persulfate is attributed to the cation exchange capacity of the Borden aquifer material which results in Na^+ attenuation (Sra et al. 2013a).

The maximum row-averaged persulfate or Na^+ concentration observed at Row 2 was approximately 0.5 g/L. The maximum concentration observed at a single sampling point was approximately 3 g/L for persulfate and approximately 0.8 g/L for Na^+. The much lower persulfate and Na^+ concentration observed at Row 2 compared to the average concentrations observed in the CIS wells (8.3 g/L for persulfate and 1.8 g/L for Na^+) indicates that significant mixing occurred between the injected solution and ambient groundwater, and perhaps some persulfate decomposed as a result of reactions with BTX compounds and aquifer materials.

Phase 3—Extended Monitoring (Day 180 to Day 391)

By Day 221, the persulfate concentration at Row 2 (Figure 4b) was below the method detection limit (MDL) indicating that the ChemOx zone had dissipated and/or migrated downgradient of this monitoring row. The persulfate decomposition in the ChemOx zone led to a significant increase in the row-averaged sulfate (SO_4^{2-}) concentrations at Row 2 shortly after persulfate injection (Figure 4b). The increased SO_4^{2-} concentration at Row 2 was first observed on Day 180 and peaked on Day 208. The produced SO_4^{2-} plume passed Row 2 and reached Row 3 by Day 221. The mass ratio between SO_4^{2-} and Na^+ was estimated based on the peak row-averaged concentration of these two compounds at Row 2. The consistency between the estimated ratio (~4) and the theoretical stoichiometry (4.2 g SO_4^{2-} per 1 g of Na^+) confirms the near complete decomposition of persulfate.

Oxidation of BTX by persulfate, if it proceeds to complete mineralization, leads to production of dissolved $CO_{2(aq)}$ and hydrogen ions (H^+), which in turn is expected to elevate DIC concentrations and decrease pH. Figure 5e and 5d shows an increased DIC concentration and a decreased pH at Row 2 which supports the occurrence of chemical oxidation. The pH at Row 2 returned to ambient levels by Day 221 due to the high buffering capacity of the calcite-rich Borden aquifer. The increased Ca^{2+} concentrations at Row 2 (Figure 5f), illustrates that the pH drop enhanced calcite dissolution, which led to buffering of the pH. Thus, it is likely that the observed peak in DIC concentration at Row 2 on Day 196 (Figure 5e) is the mixed effect of $CO_{2(aq)}$ production during BTX and NOM mineralization as well as the generation of HCO_3^- from the pH-buffering calcite dissolution reaction. The decreased BTX concentrations (Figure 4a), depletion of persulfate and production of SO_4^{2-} (Figure 4b), significant increase of EC, Eh, and DIC (Figure 5b, 5c, and 5e), as well as the drop of pH (Figure 5d), are clear geochemical indicators of persulfate oxidation of BTX at Row 2.

Unlike Row 2, the persulfate concentration at Row 3 was negligible (i.e., <MDL). Elevated Na^+ was not observed at Row 3 until Day 208 at a concentration much lower (10 to 20 times) than that observed at Row 2, likely due to dispersive mixing and/or loss in cation exchange reactions (Dance and Reardon 1983). The decreasing BTX concentrations between Day 180 and Day 208 are consistent with the BTX concentrations observed at Row 2 approximately 20 d earlier subjected to the transport and attenuation processes occurring in the system. The changes in EC, Eh, and pH were also minimal at Row 3 (Figure 5b to 5d) indicating that persulfate and thus the ChemOx zone did not reach Row 3. Instead, Row 3 captured the EBR zone as expected in the conceptual design. The increased SO_4^{2-} concentration at Row 3 which started on Day 208 and peaked on Day 221 confirmed the potential for the EBR zone. There is good agreement between the observed delay in the SO_4^{2-} plume (Figure 4d) and the geochemical indicators (e.g., EC, pH and Ca^{2+}) at Row 3 (Figure 5b, 5d, and 5f) and the expected travel time between Row 2 and Row 3.

Impact on Microbial Processes

While BTX concentrations constantly diminished during Phase 3 at Row 1, anaerobic physiological processes prevailed, as shown by diminishing concentrations of benzylsuccinates and undetectable biomarkers unique to aerobic metabolism (Figure 6a, 6d, and 6g). Interestingly, there was a spike in the concentration of phenol (produced via multiple physiological pathways), on Day 391 at Row 1, indicating a generally high biodegradation level for aromatic compounds.

Between Day 170 to Day 208, while persulfate was present at Row 2, the concentration of the majority of metabolites and the number of copies of *bssA* gene transcripts associated with anaerobic biodegradation of BTX compounds decreased

(Figure 6e, Table S2). There was also a pronounced reduction in the concentration of sulfide (the primary by-product of microbial sulfate reduction) during this period (Figure 4b). These observations indicate an inhibitory effect of persulfate on metabolic activity of the indigenous microbial community. However, this inhibition of microbial processes at Row 2 was short-term: once persulfate was depleted, the concentration of anaerobic metabolites and the number of the both *bssA*-SRB and *dsrB* expressed functional gene copies started to rebound after Day 208 (Figure 6e and 6h). The numbers of mRNA copies of *bssA-SRB* (an index of sulfate-reduction-based toluene and xylene metabolism) at Row 2 rose from below detection (~100 copies/L) to nearly 3500/L by Day 293. After Day 208, the concentration of 2-methylbenzylsuccinate rose in Row 2. Dramatically in Row 2, copies of *dsrB* mRNA rose from below detection (~100 copies/L) on Day 208 to 1.1×10^7 on Day 293 (Figure 6e) indicating an immense stimulation of sulfate-reduction activity. At the midpoint of field-monitoring efforts, the concentration of" metabolically ambiguous" (either aerobic or anaerobic) metabolites, phenol and benzoate, generally increased in Row 2 to levels far higher than baseline values; then after Day 208, concentrations fell drastically (by Day 293) only to rebound somewhat by Day 391 (Figure 6h). Beyond Day 293 at Row 2, there were spikes in the concentration of the aerobic metabolites (dimethyl phenol [from xylene], o-cresol [from toluene]), as well as in the abundance of TodC dioxygenase transcripts, perhaps indicating input of aerobic water entering the gate.

The rebound and stimulation of anaerobic microbial processes at Row 2 was concurrent with a rise in the S^{2-} concentration (Figure 4b) and DIC levels (Figure 5e) between Day 208 to Day 221. The occurrence of sulfate reduction is also supported by the isotope data on sulfate (i.e., $\delta^{34}S$ and $\delta^{18}O$). The typical trend for this process is that the remaining sulfate becomes enriched in the heavy isotopes (^{34}S and ^{18}O) as the sulfate concentration decreases. At Row 2 the sulfate representing pre-persulfate injection conditions is characterized by a concentration of approximately 7 mg/L, and $\delta^{34}S$ and $\delta^{18}O$ of 3.8 and 2.6‰, respectively. Following persulfate injection, at Day 208, the sulfate generated by the persulfate decomposition reached a concentration of approximately 1300 mg/L and showed values of 1.3 and 6.3‰ for $\delta^{34}S$ and $\delta^{18}O$, respectively (Figure 7). Between Day 208 to Day 221, the sulfate showed a decrease in concentration (~600 g/L) but no change in isotope values are observed indicating that most of the sulfate decrease was due to dilution by mixing with upgradient groundwater. During Day 221 to Day 293 a large isotopic enrichment is observed reaching values as 17.9 and 16.1‰ for $\delta^{34}S$ and $\delta^{18}O$. This isotope shift is accompanied with a decrease of sulfate from 700 to 20 mg/L (Figure 7) and these trends are typical for sulfate reduction. Later between Day 293 and Day 391, a trend to lower $\delta^{34}S$ and $\delta^{18}O$ values is observed but still these values are much higher than the pre-persulfate injection conditions (Figure 7). This trend is attributed to the mixing of groundwater containing sulfate affected and nonaffected by sulfate reduction.

These geochemical observations qualitatively confirm that microbial sulfate reduction occurred in Row 2 during this period. The eventual enhanced microbial activity (TX

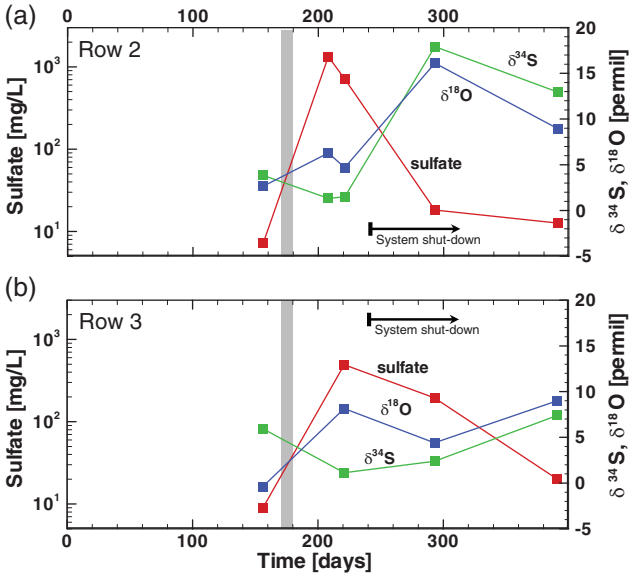

Figure 7. Sulfate concentration, and ^{34}S and ^{18}O values between Day 156 and Day 391 at approximately 2.6 m bgs at (a) Row 2 (middle ML) and (b) Row 3 (middle ML). The gray band between Day 170 and Day 180 indicates the chemical oxidation phase (Phase 2).

biodegradation and sulfate reduction) at Row 2 after an approximately 40 d inhibition period can likely be attributed to: (1) existence of subsurface heterogeneities leading to different levels of microbial exposure to persulfate; (2) dormancy, followed by growth, of indigenous microbes after persulfate concentrations diminished; (3) re-inoculation of microbial communities by upgradient groundwater; (4) increased SO_4^{2-} concentrations; and (5) enhanced biodegradability of the remaining contaminant pool following persulfate treatment causing breakdown of BTX compounds into simpler organic substrates (Gieg et al. 2014).

Patterns in the occurrence of metabolites and functional genes at Row 3 (which sampled the EBR zone) were completely different from those in Row 2 (which sampled the ChemOx zone). In the early portion of Phase 3 between Day 170 and Day 208 some traces of the *cis*-dihydrodiol aerobic metabolites were found in Row 3, before declining (Figure 6c; Table S3). More importantly, while mRNA transcripts and metabolites were suppressed in Row 2 immediately after persulfate delivery on Day 170 (Figure 6b, 6e, and 6h), in Row 3 the number of copies of the *bssA-SRB* and *dsrB* genes rose to relatively high levels from Day 190 to Day 208 (Figure 6f; Table S3), supported by sustained moderate concentrations of 2-methylbenzylsuccinate through to Day 292. This confirms the stimulation of sulfate-reduction-based biodegradation downgradient of the ChemOx zone at Row 3 which reached a lower peak SO_4^{2-} concentration of 580 mg/L compared to the peak concentration of 1430 mg/L at Row 2 (Figure 4b). We acknowledge that spatially dependent mixing and transport processes may have contributed to the low sulfate concentrations found at Row 3.

Besides featuring benzylsuccinate metabolites, *bssA-SRB* and *dsrB* transcripts, consumption of sulfate, and elevated sulfide concentrations, the stimulated EBR zone at Row 3 also showed elevated concentrations of the "metabolically

ambiguous" (either aerobic or anaerobic) metabolites, phenol and benzoate (Figure 6i). As seen for Rows 1 and 2, there was a spike in the concentration of the aerobic xylene metabolite, dimethyl phenol (as well as aerobic toluene metabolite, *o*-cresol), on Day 391 in Row 3, perhaps due to input of aerobic water entering the gate. No clear evidence of sulfate reduction as revealed at Row 2 is observed from the sulfate isotope data gathered from Row 3. These data showed isotope values at the high sulfate peak of approximately 500 mg/L not too different than the sulfate produced by the persulfate decomposition at Row 2 (Figure 7). Then as the sulfate concentration decreases, $\delta^{34}S$ values tend toward enriched values but not the $\delta^{18}O$ values. The larger isotopic enrichment indicative of sulfate reduction is observed between Day 293 and Day 391 when the sulfate decreases from about 200 to 20 mg/L, and the isotope values increases from 2.4 to 7.4‰ for $\delta^{34}S$, and from 4.4 to 9.0‰ for $\delta^{18}O$. The primary reason for the different isotope pattern observed at Row 3 compared to Row 2 is related to groundwater flow. The isotopic fractionation induced by microbial sulfate reduction at Row 3 may be masked due to dispersive mixing with transported sulfate generated by persulfate decomposition which is characterized by depleted $\delta^{34}S$ and $\delta^{18}O$ values. Overall, we interpret the above multiple lines of data as clear evidence for sulfate-enhanced TX biodegradation.

Reactive Zone Characterization Using CSIA Data

The geochemical and molecular biological data clearly show the occurrence of the two successive reactive zones: chemical oxidation controls mass reduction in the ChemOx zone, while enhanced microbial sulfate reduction dominates the mass loss in the downgradient EBR zone. In other dynamic systems, however, this separation of mass removal processes may not be as easy to demonstrate. Due to groundwater flow, many of the changes occurring in the ChemOx zone could be reflected in the EBR zone with a lag-time (controlled by groundwater velocity) which alters the signature of the distinct processes occurring in the downgradient EBR zone. To overcome these potential complications, the coupling of the $\delta^{13}C$ and $\delta^{2}H$ data using the dual element isotope approach provides complementary information that can be used to evaluate the occurrence and ability to differentiate the two reactive zones.

For example, Figure 8 was prepared using the temporal isotopic data for benzene (Figure S5) in conjunction with the dual carbon and hydrogen isotope slopes reported in the literature for persulfate oxidation, and aerobic and anaerobic biodegradation of benzene (Solano et al. 2017). In this figure, $\Delta\delta^{13}C$ and $\Delta\delta^{2}H$ respectively represent the change in the carbon and hydrogen isotope ratios from time zero (in the source solution) to time *t*. The $\Delta\delta^{13}C$ and $\Delta\delta^{2}H$ data clearly demonstrate a distinct evolution of the isotopic fractionation pattern at Row 2 and Row 3.

At Row 2 (Figure 8a), the observed $\Delta\delta^{13}C-\Delta\delta^{2}H$ data from Day 170 to Day 208 are close to the line representing the isotopic fractionation of benzene associated with persulfate oxidation (Solano et al. 2017). This observation confirms that persulfate oxidation was the dominant mass removal process at Row 2 during this period. Starting from Day 221, a deviation from the persulfate oxidation line toward

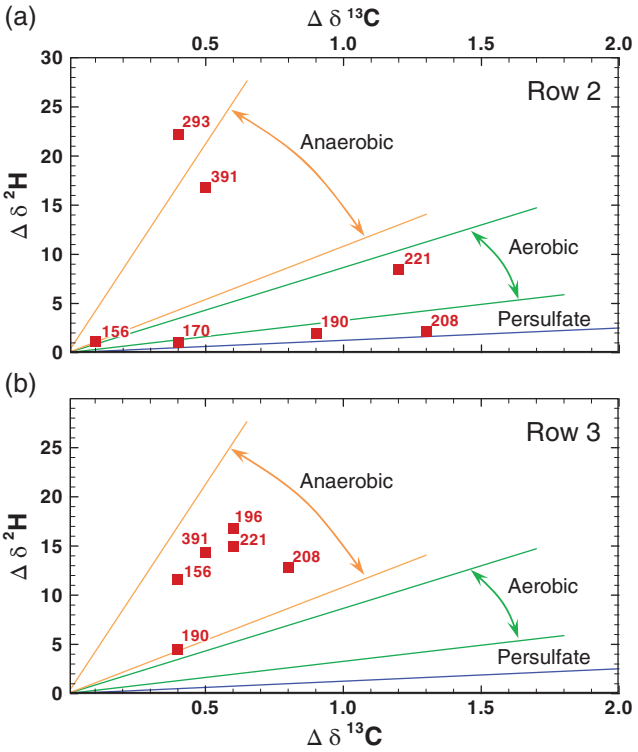

Figure 8. Two-dimensional CSIA representation of the C/H isotope fractionation data for benzene at approximately 2.6 m bgs at (a) Row 2 (left ML) and (b) Row 3 (middle ML). The corresponding sampling time (Day) is adjacent to each data point. The green and orange regions represent the range of $\Delta\delta^{13}C$ to $\Delta\delta^{2}H$ values reported in the literature for aerobic and anaerobic biodegradation of benzene, respectively. The blue line represents the $\Delta\delta^{13}C$ to $\Delta\delta^{2}H$ values corresponding to benzene oxidation by persulfate. See Solano et al. (2017) for details.

the anaerobic biodegradation area was observed which was likely due to the depletion of persulfate and enhanced microbial sulfate reduction. From Day 221 to Day 293 the system was shut-down for winter and significant isotopic shifts were observed indicating anaerobic biodegradation. The isotopic data for toluene and xylene followed a similar evolution pattern (Figures S6 and S7).

For Row 3 (Figure 8b) however, the clustering of $\Delta\delta^{13}C-\Delta\delta^{2}H$ data in the area representing anaerobic biodegradation suggests that anaerobic biodegradation was the predominant mass removal process at this location. The slightly depleted isotope signature observed at Row 3 on Day 190 corresponds to the arrival of oxidized groundwater from Row 2 due to the ongoing transport (Figure 5b).

Mass Loss Estimation

In an attempt to evaluate the treatment effectiveness following persulfate addition, the BTX mass loss was estimated between Day 150 and Day 221 using the BTX concentration data. First, the mass loading at Rows 1, 2, and 3 was estimated by integrating the product of the row-averaged BTX concentrations, Darcy flux and the cross-sectional area of the gate. Second, the cumulative mass loading profiles for each row were estimated by integrating the mass loading over time. Third, the cumulative mass loading profiles for Row 2 and Row 3 were shifted in time to account for the transport

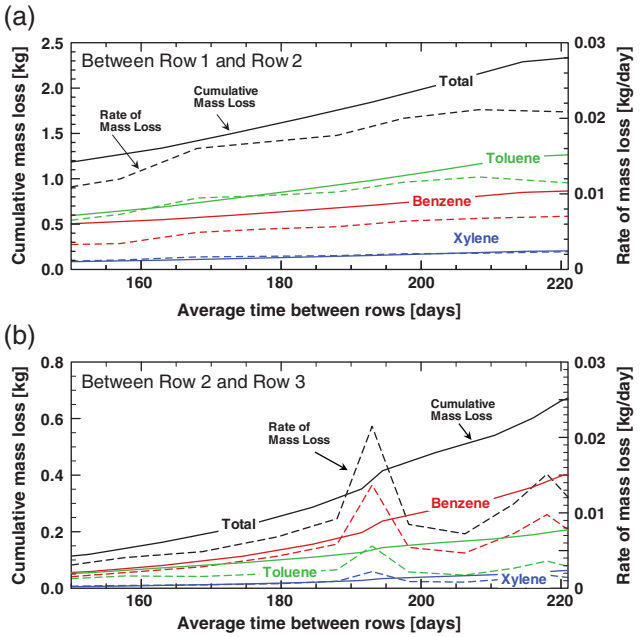

Figure 9. Cumulative mass loss (solid lines) and mass loss rate (dashed lines) between (a) Row 1 and Row 2, and (b) Row 2 and Row 3 from Day 150 to Day 221.

between rows. Finally, assuming no mass accumulation occurred between rows, the difference between the cumulative mass loading profiles was used to estimate the mass lost. For these calculations, a velocity of 15 cm/d was used or a travel time of 20 d between rows. This mass loss estimation approach cannot differentiate the contribution of individual mass removal processes (e.g., persulfate oxidation, biodegradation) to the total mass loss. Quantifying the uncertainties and interpolation errors associated with this mass loss estimate is difficult but they are thought to be about ±50% according to Schirmer et al. (2000). The cumulative mass loss and the mass loss rate (i.e., mass loss per unit time, or slope of the cumulative mass loss profile) between Row 1 and Row 2, and between Row 2 and Row 3 are presented in Figure 9.

The total BTX mass loss from Day 150 and Day 221 between Row 1 and Row 2 was approximately 1.2 kg (Figure 9a). The highest mass loss was for toluene (~0.7 kg), followed by benzene (0.4 kg) and xylene (0.1 kg). The rate of BTX mass removal appears to be relatively constant (6 x 10^{-3} kg/d for benzene, 1x10^{-2} kg/d for toluene, and 2x10^{-3} kg/d for xylene) between Day 150 and Day 221. Surprisingly the impact of the persulfate injections between Row 1 and Row 2 is not apparent in these data despite the minor decrease in BTX concentration observed at Row 2 (Figure 4a). Likely the method used to estimate this mass loss resulted is some data smoothing that removed these finer-scale features. According to the molecular biological data, microbial processes were inhibited at Row 2 due to the presence of persulfate, and chemical oxidation was identified by CSIA as a mass removal process in the vicinity of Row 2. Notwithstanding this observation, the majority of the mass loss between Row 1 and Row 2 can be attributed to the biodegradation processes established during the plume development phase.

In contrast to the mass loss between Row 1 and Row 2, the mass loss between Row 2 and Row 3 shows two pronounced occurrences when the rate of mass loss increased. The first occurs about Day 190 and is related to the ChemOx zone as it moves downgradient from Row 2, while the second occurs about Day 215 and is associated with the establishment of the EBR zone between Row 2 and Row 3. The CSIA and molecular biological data (Figures 6 and 8) support the dominant mass removal progresses associated with the presence of these two occurrences. The total BTX mass loss from Day 150 to Day 221 between Row 2 and Row 3 was approximately 0.6 kg, with benzene having the highest mass loss followed by toluene and xylene.

The mass loss estimates discussed above are reflective of the BTX plumes subjected to two persulfate injection pulses purposely designed to degrade only a portion of the BTX mass. At an actual site, it is expected that the mass removal by chemical oxidation would be substantially larger than observed in this investigation.

Stopped Flow Conditions

Groundwater extraction and the feed to the source wells were stopped on Day 221 due to unfavorable winter conditions; however, monitoring and sampling were performed on Day 293 and Day 391. The stopped flow condition was expected to: (1) decrease BTX concentrations due to the system shutdown and ongoing biodegradation, and (2) prevent further migration of the elevated sulfate plume. Thus, this flow shutdown would limit the spatial extent of the enhanced sulfate reduction zone and consequently lead to biodegradation pathways other than sulfate reduction. When the system was shutdown, the advective front of the EBR zone was estimated to be between Row 3 and Row 4, and hence no significant enhanced biogeochemical changes were observed at Rows 4 to 6 (Figures 4 and 5). The observed sulfate breakthrough at Row 4 on Day 293 is attributed to dispersion and then diffusion. By Day 391, due to the system shut down and sustained microbial processes, toluene and xylene were preferentially removed from the gate relative to benzene which remained elevated at approximately 1000 µg/L (Figure 4). Between Day 221 and Day 391, the geochemical indicators (e.g., ORP, pH, EC, and DO) remained unchanged but SO_4^{2-}, S^{2-}, Ca^{2+} and DIC concentrations decreased at both Row 2 and Row 3. Figure 8 clearly shows the shift of the dominant mass removal process from chemical oxidation (before Day 221) to anaerobic biodegradation (after Day 221) at Row 2, while anaerobic biodegradation remained the primary mass removal process at Row 3. While this stopped flow condition is not representative of conditions at other sites, the interpretation of the monitoring data (particularly the CSIA and molecular biological data) provide insights into changes in the underlying biodegradation pathways.

Transition to Methanogenesis

The stopped flow conditions from Day 221 to Day 391 caused the balance between the electron donor (e.g., BTX) and acceptor (e.g., sulfate) that governs microbial metabolism to shift resulting in methanogenic metabolism (e.g., use of carbon dioxide as electron acceptor) since the microbial respiratory demand was high and sulfate supply was low. Elevated methane concentrations were found at Row 3 on Day 293 and Day 391 (~100 µg/L), and at Row 2 on Day 391

(~50 µg/L; Figure S8), indicating that methanogenesis began earlier and was more extensive in Row 3 (most distant from the persulfate source) than in Row 2.

Trends in biomarker analyses indicated that microbial populations in Rows 2 and 3, indeed, underwent a transition from sulfate-reducing conditions toward something else. The definitive way to positively identify a transition to methanogenesis would have been to monitor mRNA transcripts from the *mcrA* gene (characteristic of active methanogens) throughout this study, noting a drastic rise at the end; unfortunately this assay was not completed. Instead, we offer a simple inverse relationship between geochemically monitored methane production (see above) and biomarkers of sulfate reduction activity. Abundances of mRNA copies of both *dsrB* and *bssA-SRB* genes dropped strikingly (below detection) at Row 3 on Days 221, 293, and 391, when methanogenesis was highest (Figure 6f). Also, on the same 3 d in Row 2 (with less methanogenesis and later onset), counts of mRNA copies/L of *dsrB* and *bssA-SRB* genes were 153, 1.1×10^7, 5.5×10^5 and 180, 3500, and <MDL, respectively.

Consistent with both recent and past views about the anaerobic physiology of BTX biodegradation (e.g., Fuchs et al. 2011; Fowler et al. 2012; Grbić-Galić and Vogel 1987; Lovley and Lonergan 1990; Evans et al. 1992; Zhang et al. 2013, 2014), both carboxylation and hydroxylation have been reported under anaerobic (especially, methanogenic and iron-reducing) conditions. Such reactions are fully consistent with the production of dimethylphenol, phenol, *o*-cresol and benzoate which were found at relatively high concentrations in the late stage of Phase 3 at Rows 2 and 3 (Figure 6, Table S3). Thus, the geochemical and biomarker data are consistent regarding the mechanism of transition from a sulfate-reducing to a methanogenic regime.

Closure

Multiple lines of evidence assembled in this experiment demonstrated that chemical oxidation was the dominant mass removal process in the vicinity of the persulfate injections (i.e., ChemOx zone), while EBR (including enhanced microbial sulfate reduction and methanogenesis) dominated BTX degradation in the downgradient portions of the plume (i.e., EBR zone).

Stable isotope analyses of BTX and sulfate, and monitoring of process-specific functional genes and intermediate metabolites provided essential data used to identify the dominant mass removal processes. CSIA data clearly indicated the spatial and temporal separation of the ChemOx and EBR zones. The coupling of $\delta^{13}C$ and $\delta^{2}H$ data demonstrated a distinct and specific isotopic trend for chemical oxidation and anaerobic biodegradation processes, which respectively dominated the mass removal in the ChemOx and EBR zones. The sulfur and oxygen isotope data for sulfate qualitatively confirmed the occurrence of microbial sulfate reduction in the ChemOx zone following persulfate injection and the EBR zone. Molecular biology data demonstrated the short- and long-term impact of persulfate on the population and biodegradation activity of indigenous microbial communities including SRB. The decreased concentration of anaerobic metabolites such as benzylsuccinate, 2-MeBS and benzoate, and reduced number of the expressed *bssA-SRB* genes associated with BTX anaerobic biodegradation indicated that persulfate, even at low concentrations (<10 g/L), caused a temporary inhibition of microbial processes in the ChemOx zone. However, the concentration of metabolites and the number of copies of the *bssA-SRB* and *dsrB* genes (the latter being associated with BTX degradation under sulfate reduction) increased significantly after persulfate depletion. The incomplete inhibition of microbial processes is presumably due to the low dosage and short duration of the persulfate treatment, existence of subsurface heterogeneities and persistence/growth of indigenous microbes in the dead-end pores, reinoculation of microbial communities by groundwater flow, and increased sulfate concentration contributed to the observed enhancement of the microbial sulfate reduction following persulfate delivery. Transport of microbial communities, sulfate, nutrients and bioavailable substrates not only facilitates the natural rebound of indigenous microbial communities but also defines the dominant biodegradation pathway.

Based on the findings from this pilot-scale investigation, a combined persulfate/EBR system appears to be feasible alternative for treatment of PHC plumes; however, the balance between the persulfate dose and the ability of the system to then enhance biodegradation is the key to successful implementation. While the findings discussed in this paper provide an indication of the opportunities of a combined persulfate/EBR system, insights into the engineering controls to achieve optimal system behavior are not provided. Ongoing efforts using the data generated from this study in combination with an appropriate simulation model will provide these insights and related guidance.

Acknowledgments

We thank Kammy Sra for his valuable comments on this manuscript. Financial support for this investigation was provided by Chevron Energy Technology Company, American Petroleum Institute (API), and a NSERC of Canada Collaborative Research and Development Grant (N.R.T.).

Supporting Information

The following supporting information is available for this article:

Appendix S1: Analytical Methods

Figure S1. (a) Image of the experimental gate; (b) installation of Waterloo Emitters inside the source wells; and (c) CIS wells located between Row 1 and Row 2.

Figure S2. Timeline of the pilot-scale experiment, and the frequency of monitoring and groundwater sampling episodes.

Figure S3. Temporal evolution of groundwater depth (▼) and velocity (▶) in the experimental gate, and the average total BTX concentration in the source tanks (red ■) and wells (green ■). The solid pink line between Day 15 and Day 45 indicates the average velocity supported by the tracer test data.

Figure S4. Row-averaged (based on weighted cross-sectional area) persulfate and sodium concentrations at Row 2.

Figure S5. Carbon and hydrogen isotope data of benzene at approximately 2.6 m bgs for (a) Row 2 (left ML2-L3) and (b) Row 3 (middle ML3-M3).

Figure S6. Carbon and hydrogen isotope data of toluene at approximately 2.6 m bgs for (a) Row 2 (left ML2-L3) and (b) Row 3 (middle ML3-M3).

Figure S7. Carbon and hydrogen isotope data of xylene at approximately 2.6 m bgs for (a) Row 2 (left ML2-L3) and (b) Row 3 (middle ML3-M3).

Figure S8. Row-averaged methane concentrations at Row 2 and Row 3 on Day 293 and Day 391. Higher methane concentrations at Row 3 suggest a greater role of methanogenesis over sulfate reduction at this location compared to Row 2.

Table S1. (a) Process-specific key intermediate metabolites used in assessment of in situ biodegradation. (b) Monitored functional genes (detected as expressed mRNA) that are diagnostic of in situ biodegradation.

Table S2. PCR primers.

Table S3. Patterns in the occurrence of copies of mRNA transcripts of (a) functional genes and (b) key metabolites at Row 2 and Row 3.

References

Abu Laban, N., D. Selesi, T. Rattei, P. Tischler, and R.U. Meckenstock. 2010. Identification of enzymes involved in anaerobic benzene degradation by a strictly anaerobic iron-reducing enrichment culture. *Environmental Microbiology* 12, no. 10: 2783–2796.

Acton, D.W., and J.F. Barker. 1992. In situ biodegradation potential of aromatic hydrocarbons in anaerobic groundwaters. *Journal of Contaminant Hydrology* 9, no. 4: 325–352.

Arildskov, N.P., and J.F. Devlin. 2000. Field and laboratory evaluation of diffusive emitter for semipassive release of PCE to an aquifer. *Groundwater* 38, no. 1: 129–138.

Beller, H.R., S.R. Kane, T.C. Legler, J.R. McKelvie, B.S. Lollar, F. Pearson, L. Balser, and D.M. Mackay. 2008. Comparative assessments of benzene, toluene, and xylene natural attenuation by quantitative polymerase chain reaction analysis of a catabolic gene, signature metabolites, and compound-specific isotope analysis. *Environmental Science & Technology* 42, no. 16: 6065–6072.

Beller, H.R., A.M. Spormann, P.K. Sharma, J.R. Cole, and M. Reinhardet. 1996. Isolation and characterization of a novel toluene-degrading, sulfate-reducing bacterium. *Applied and Environmental Microbiology* 62, no. 4: 1188–1196.

Bolliger, C., P. Höhener, D. Hunkeler, K. Häberli, and J. Zeyer. 1999. Intrinsic bioremediation of a petroleum hydrocarbon-contaminated aquifer and assessment of mineralization based on stable carbon isotopes. *Biodegradation* 10, no. 3: 201–217.

Bou-Nasr, J., D. Cassidy, and D. Hampton. 2006. Comparative study of the effect of four ISCO oxidants on PCE oxidation and aerobic microbial activity. In *Proceedings of the Fifth International Conference on Remediation of Chlorinated and Recalcitrant Compounds*. Monterey, CA. Columbus, Ohio: Battelle Press.

Bourne, D.G., A. Muirhead, and Y. Sato. 2011. Changes in sulfate-reducing bacterial populations during the onset of black band disease. *ISME Journal* 5, no. 3: 559–564.

Cassidy, D., A. Northup, and D. Hampton. 2009. The effect of three chemical oxidants on subsequent biodegradation of 2,4-dinitrotoluene (DNT) in batch slurry reactors. *Journal of Chemical Technology & Biotechnology* 84, no. 6: 820–826.

Cassidy, D. 2008. *The Effect of Klozur® CR on Sulfate-Reducing Bacteria (SRB) in Sediments from the Kalamazoo River*. FMC Environmnetal Solutions Peroxygen Talk series. Philadelphia, Pennsylvania.

Cébron, A., M.P. Norini, T. Beguiristain, and C. Leyval. 2008. Real-time PCR quantification of PAH-ring hydroxylating dioxygenase (PAH-RHDα) genes from gram positive and gram negative bacteria in soil and sediment samples. *Journal of Microbiology Methods* 73, no. 2: 148–159.

Chin, K.J., M.L. Sharma, L.A. Russell, K.R. O'Neill, and D.R. Lovley. 2008. Quantifying expression of a dissimilatory (bi)sulfite reductase gene in petroleum-contaminated marine harbor sediments. *Microbial Ecology* 55, no. 3: 489–499.

Cunningham, J.A., H. Rahme, G.D. Hopkins, C. Lebron, and M. Reinhard. 2001. Enhanced in situ bioremediation of BTEX-contaminated groundwater by combined injection of nitrate and sulfate. *Environmental Science & Technology* 35, no. 8: 1663–1670.

Dance, J.T., and E.J. Reardon. 1983. Migration of contaminants in groundwater at a landfill: A case study. *Journal of Hydrology* 63, no. 1–2: 109–130.

Devlin, J.F., D. Katic, and J.F. Barker. 2004. In situ sequenced bioremediation of mixed contaminants in groundwater. *Journal of Contaminant Hydrology* 69, no. 3–4: 233–261.

Devlin, J.F., and J.F. Barker. 1996. Field investigation of nutrient pulse mixing in an in situ biostimulation experiment. *Water Resources Research* 32, no. 9: 2869–2877.

Diaz, E., J.I. Jiménez, and J. Nogales. 2013. Aerobic degradation of aromatic compounds. *Current Opinion in Biotechnology* 24, no. 3: 431–442.

Droste, E.X., M.C. Marley, J.M. Parikh, A.M. Lee, P.M. Dinardo, B.A. Woody, G.E. Hoag, and P. Chedda. 2002. Observed enhanced reductive dechlorination after in situ chemical oxidation pilot test. In *Proceedings of the Third International Conference on Remediation of Chlorinated and Recalcitrant Compounds*. Monterey, CA. Columbus, Ohio: Battelle Press.

Evans, P.J., W. Ling, B. Goldschmidt, E.R. Ritter, and L.Y. Young. 1992. Metabolites formed during anaerobic transformation of toluene and o-xylene and their proposed relationship to the initial steps of toluene mineralization. *Applied and Environmental Microbiology* 58, no. 2: 496–501.

Fowler, S.J., X. Dong, C.W. Sensen, J.M. Suflita, and L.M. Gieg. 2012. Methanogenic toluene metabolism: Community structure and intermediates. *Environmental Microbiology* 14, no. 3: 754–764.

Fuchs, G., M. Boll, and J. Heider. 2011. Microbial degradation of aromatic compounds—From one strategy to four. *Nature Review Microbiology* 9, no. 11: 803–816.

Gallagher, L., and M. Crimi. 2007. Coupling persulfate ISCO with bioprocesses: A review. In *Proceedings of the Fifth International Conference on Oxidation and Reduction Technologies for the in Situ Treatment of Soil and Groundwater*. Niagara Falls, New York.

Geets, J., B. Borremans, L. Diels, D. Springael, J. Vangronsveld, D. van der Lelie, and K. Vanbroekhoven. 2006. DsrB gene-based DGGE for community and diversity surveys of sulfate-reducing bacteria. *Journal of Microbiological Methods* 66: 194–205.

Gieg, L.M., S.J. Fowler, and C. Berdugo-Clavijo. 2014. Syntrophic biodegradation of hydrocarbon contaminants. *Current Opinion in Biotechnology* 27: 21–29.

Gierczak, R., J.F. Devlin, and D.L. Rudolph. 2007. Field test of a cross-injection scheme for stimulating in situ denitrification near a municipal water supply well. *Journal of Contaminant Hydrology* 89, no. 1-2: 48–70.

Grbić-Galić, D., and T.M. Vogel. 1987. Transformation of toluene and benzene by mixed methanogenic cultures. *Applied and Environmental Microbiology* 53, no. 2: 254–260.

Gülensoy, N., and P.J. Alvarez. 1999. Diversity and correlation of specific aromatic hydrocarbon biodegradation capabilities. *Biodegradation* 10, no. 5: 331–340.

Harms, G., K. Zengler, R. Rabus, F. Aeckersberg, D. Minz, R. Rosselló-Mora, and F. Widdel. 1999. Anaerobic oxidation of o-xylene, m-xylene, and homologous alkylbenzenes by new types of sulfate-reducing bacteria. *Applied and Environmental Microbiology* 65, no. 3: 999–1004.

Hendrickx, B.H., H. Junca, J. Vosahlova, A. Lindner, I. Ruegg, M. Bucheli-Witschel, F. Faber, T. Egli, M. Mau, D.H. Pieper, E.M. Top, W. Dejonghe, L. Bastiaens, and D. Springael. 2006. Alternative primer sets for PCR detection of genotypes involved in bacterial aerobic BTEX degradation: Distribution of the genes in BTEX degrading isolates and in subsurface soils of a BTEX contaminated industrial site. *Journalm of Microbiology Methods* 64, no. 2: 250–265.

Huang, K.C., Z. Zhao, G.E. Hoag, A. Dahmani, and P.A. Block. 2005. Degradation of volatile organic compounds with thermally activated persulfate oxidation. *Chemosphere* 61, no. 4: 551–560.

Huling, S.G., and B.E. Pivetz. 2006. *Engineering Issue: In-situ Chemical Oxidation*. EPA/600/R-06/072. Cincinnati, Ohio: U.S. Enviromnmental Protection Agency Office of Research and Development, National Risk Management Research Laboratory.

Hunkeler, D., R. Aravena, B.L. Parker, J.A. Cherry, and X. Diao. 2003. Monitoring oxidation of chlorinated ethenes by permanganate in groundwater using stable isotopes: Laboratory and field studies. *Environmental Science & Technology* 37, no. 4: 798–804.

Interstate Technology & Regulatory Council (ITRC). 2005. Technical/Regulatory Guideline Technical and Regulatory Guidance for In Situ Chemical Oxidation of Contaminated Soil and Groundwater, 2nd ed. Prepared by The Interstate Technology & Regulatory Council In Situ Chemical Oxidation Team. January 2005.

Kazy, S.K., A.L. Monier, and P.J.J. Alvarez. 2010. Assessing the correlation between anaerobic toluene degradation activity and bssA concentrations in hydrocarbon-contaminated aquifer material. *Biodegradation* 21, no. 5: 793–800.

Kleikemper, J., M.H. Schroth, W.V. Sigler, M. Schmucki, S.M. Bernasconi, and J. Josef Zeyer. 2002. Activity and diversity of sulfate-reducing bacteria in a petroleum hydrocarbon-contaminated aquifer. *Applied and Environmental Microbiology* 68, no. 4: 1516–1523.

Lee, B.T., and K.W. Kim. 2002. Ozonation of diesel fuel in unsaturated porous media. *Applied Geochemistry* 17, no. 8: 1165–1170.

Liang, C., C.F. Huang, and Y.J. Chen. 2008. Potential for activated persulfate degradation of BTEX contamination. *Water Research* 42, no. 15: 4091–4100.

Lovley, D.R., and D.J. Lonergan. 1990. Anaerobic oxidation of toluene, phenol, and p-cresol by the dissimilatory iron-reducing organism, GS-15. *Applied and Environmental Microbiology* 56, no. 6: 1858–1864.

MacFarlane, D.S., J.A. Cherry, R.W. Gilham, and E.A. Sudicky. 1983. Migration of contaminants in groundwater at a NDFILL: A case-groundwater flow and plume delineation. *Journal of Hydrology* 63, no. 1-2: 1–29.

Mackay, D.M., D.L. Freyberg, P.V. Roberts, and J.A. Cherry. 1986. A natural gradient experiment on solute transport in a sand aquifer: 1. Approach and overview of plume movement. *Water Resources Research* 22, no. 13: 2017–2029.

MacKinnon, L.K., and N.R. Thomson. 2002. Laboratory-scale in situ chemical oxidation of a perchloroethylene pool using permanganate. *Journal of Contaminant Hydrology* 56, no. 1-2: 49–74.

Mancini, S.A., A.C. Ulrich, G. Lacrampe-Couloume, B. Sleep, Edwards, and B.S. Lollar. 2003. Carbon and hydrogen isotopic fractionation during anaerobic biodegradation of benzene. *Applied and Environmental Microbiology* 69, no. 1: 191–198.

Marchesi, M., N.R. Thomson, R. Aravena, K.S. Sra, N. Otero, and A. Soler. 2013. Carbon isotope fractionation of 1,1,1-trichloroethane during base-catalyzed persulfate treatment. *Journal of Hazardous Materials* 260: 61–66.

Marley, M.C., J.M. Parikh, E.X. Droste, and A.M. Lee. 2006. A case study on enhanced reductive dechlorination resulting from a chemical oxidation pilot test. In *First International Conference on DNAPL Characterization and Remediation*. Pittsburgh, PA.

Miao, Z., M.L. Brusseau, K.C. Carroll, C. Carreón-Diazconti, and B. Johnsonet. 2012. Sulfate reduction in groundwater: Characterization and applications for remediation. *Environmental Geochemistry and Health* 34, no. 4: 539–550.

Morasch, B., H.H. Richnow, B. Schink, and R.U. Meckenstock. 2001. Stable hydrogen and carbon isotope fractionation during microbial toluene degradation: Mechanistic and environmental aspects. *Applied and Environmental Microbiology* 67, no. 10: 4842–4849.

Munakata-Marr, J., K. Sorenson, B. Petri, and J. Cummings. 2011. Principles of combining ISCO with other in situ remedial approaches. In *In Situ Chemical Oxidation for Groundwater Remediation*, Vol. 3, ed. R.L. Siegrist, M. Crimi, and T.J. Simpkin, 285–317. New York: Springer.

Nebe, J., B.R. Baldwin, R.L. Kassab, L. Nies, and C.H. Nakatsu. 2009. Quantification of aromatic oxygenase genes. *Environmental Science & Technology* 43, no. 6: 2029–2034.

Neretin, L.N., A. Schippers, A. Pernthaler, K. Hamann, R. Amann, and B.B. Jørgensen. 2003. Quantification of dissimilatory (bi) sulphite reductase gene expression in Desulfobacterium autotrophicum using real-time RT-PCR. *Environmental Microbiology* 5, no. 8: 660–671.

Nicholson, R.V., J.A. Cherry, and E.J. Reardon. 1983. Migration of contaminants in groundwater at a landfill: A case study. 6. Hydrogeochemistry. *Journal of Hydrology* 63, no. 1-2: 131–176.

Pelikan, C., C.W. Herbold, B. Hausmann, A.L. Müller, M. Pester, and A. Loy. 2016. Diversity analysis of sulfite- and sulfate-reducing microorganisms by multiplex dsrA and dsrB amplicon sequencing using new primers and mock community-optimized bioinformatics. *Environment Microbiology* 18, no. 9: 2994–3009. https://doi.org/10.1111/1462-2920.13139

Poulson, S.R., and H. Naraoka. 2002. Carbon isotope fractionation during permanganate oxidation of chlorinated ethylenes (cDCE, TCE, PCE). *Environmental Science & Technology* 36, no. 15: 3270–3274.

Reinhard, M., S. Shang, P.K. Kitanidis, E. Orwin, G.D. Hopkins, and C.A. Lebron. 1997. In situ BTEX biotransformation under enhanced nitrate- and sulfate-reducing conditions. *Environmental Science & Technology* 31, no. 1: 28–36.

Richardson, S.D., B.L. Lebron, C.T. Miller, and M.D. Aitken. 2011. Recovery of phenanthrene-degrading bacteria after simulated in situ persulfate oxidation in contaminated soil. *Environmental Science & Technology* 45, no. 2: 719–725.

Sahl, J.W., J. Munakata-Marr, M.L. Crimi, and R.L. Siegrist. 2007. Coupling permanganate oxidation with microbial dechlorination of tetrachloroethene. *Water Environment Research* 79, no. 1: 5–12.

Sahl, J., and J. Munakata-Marr. 2006. The effects of in situ chemical oxidation on microbiological processes: A review. *Remediation Journal* 16, no. 3: 57–70.

Schirmer, M., J.W. Molson, E.O. Frind, and J.F. Barker. 2000. Biodegradation modelling of a dissolved gasoline plume applying independent laboratory and field parameters. *Journal of Contaminant Hydrology* 46, no. 3-4: 339–374.

Sessa, F., J. Paré, and J.E. Studer. 2008. Coupled ISCO-bio via activated persulfate and timed oxygen release using a sodium persulfate/calcium peroxide matrix. In *Proceeding of the Remediation Technologies Symposium 2008 (RemTech 2008)*. Banff, Canada.

Solano, F.M., M. Marchesi, N.R. Thomson, D. Bouchard, and R. Aravena. 2017. Carbon and hydrogen isotope fractionation of benzene, toluene and o-xylene during chemical oxidation by persulfate. *Groundwater Monitoring and Remediation*. https://doi.org/10.1111/gwmr.12228

Sra, K.S., N.R. Thomson, and J.F. Barker. 2013a. Persulfate injection into a gasoline source zone. *Journal of Contaminant Hydrology* 150: 35–44.

Sra, K.S., N.R. Thomson, and J.F. Barker. 2013b. Persulfate treatment of dissolved gasoline compounds. *Journal of Hazardous, Toxic, and Radioactive Waste* 17, no. 1: 9–15.

Sra, K.S., N.R. Thomson, and J.F. Barker. 2010. Persistence of persulfate in uncontaminated aquifer materials. *Environmental Science & Technology* 44, no. 8: 3098–3104.

Studer, J., G. Davis, B. Baldwin, and G. Cronk. 2009. Impact of in situ chemical oxidation on native biological populations: Review of case studies. In *Proceeding of the Tenth International in Situ and on-Site Bioremediation Symposium*. Battelle, Baltimore.

Sutton, N.B., J.T.C. Grotenhuis, A.A.M. Langenhoff, and H.H.M. Rijnaarts. 2010. Efforts to improve coupled in situ chemical oxidation with bioremediation: A review of optimization strategies. *Journal of Soils and Sediments* 11: 129–140.

Thomson, N.R., M. Fraser, C. Lamarche, J. Barker, and S. Forsey. 2008. Rebound of a creosote plume following partial source zone treatment with permanganate. *Journal of Contaminant Hydrology* 102, no. 1-2: 154–171.

Tsitonaki, A., B.F. Smets, and P.L. Bjerg. 2008. Effects of heat-activated persulfate oxidation on soil microorganisms. *Water Research* 42, no. 4-5: 1013–1022.

U.S. Environmental Protection Agency (U.S. EPA). 2013. *Introduction to In Situ Bioremediation of Groundwater*. EPA 542-R-13-018. Office of Solid Waste and Emergency Response (accessed December 2015).

Whited, G.M., and D.T. Gibson. 1991. Toluene-4-monooxygenase, a three-component enzyme system that catalyzes the oxidation of toluene to p-cresol in Pseudomonas Mendocina KR1. *J. Bacteriol* 173: 3010–3016.

Wilson, M.S., and E.L. Madsen. 1996. Field extraction of a unique intermediary metabolite indicative of real time in situ pollutant biodegradation. *Environmental Science & Technology* 30, no. 6: 2099–2103.

Wilson, R.D., and D.M. Mackay. 1995a. A method for passive release of solutes from an unpumped well. *Groundwater* 33: 936–945.

Wilson, R.D., and D.M. Mackay. 1995b. A method for passive release of solutes from an unpumped well. *Groundwater* 33: 936–945.

Xu, X., and N.R. Thomson. 2009. A long-term bench-scale investigation of permanganate consumption by aquifer materials. *Journal of Contaminant Hydrology* 110: 73–86.

Yang, G.C., L.C. Wu, C.S. Wu, and I.Y. Hsu. 2005. Treatment train for site remediation at a petrochemicals-contaminated site within a petroleum refinery. *Bulletin of Environmental Contamination and Toxicology* 74, no. 5: 904–912.

Zhang, Z., P.-L. Tremblay, A.K. Chaurasia, J.A. Smith, T.S. Bain, and D.R. Lovley. 2014. Identification of genes specifically required for the anaerobic metabolism of benzene in Geobacter metallireducens. *Frontiers in Microbiology* 5: 245.

Zhang, T.P.-L.T., A.K. Chaurasia, J.A. Smith, T.S. Bain, and D.R. Lovley. 2013. Anaerobic benzene oxidation via phenol in Geobacter metallireducens. *Applied and Environmental Microbiology* 79, no. 24: 7800–7806.

Biographical Sketches

Mahsa Shayan, *Ph.D., E.I.T., corresponding author, Department of Civil and Environmental Engineering, University of Waterloo, Waterloo, ON, Canada. Now at AECOM, 55 Wyndham Street North, Guelph, ON N1H 7T8, Canada; mshayanm@uwaterloo.ca.*

Neil R. Thomson, *Ph.D., P.Eng., is Professor at Department of Civil and Environmental Engineering, University of Waterloo, 200 University Ave. West, Waterloo, ON N2L 3G1, Canada.*

Ramon Aravena, *Ph.D., is Emeritus and Adjunct Professor at Department of Earth and Environmental Sciences, University of Waterloo, 200 University Ave. West, Waterloo, ON N2L 3G1, Canada.*

James F. Barker, *Ph.D., is Emeritus and Adjunct Professor at Department of Earth and Environmental Sciences, University of Waterloo, 200 University Ave. West, Waterloo, ON N2L 3G1, Canada.*

Eugene L. Madsen, *Ph.D., is Professor at Department of Microbiology, Cornell University, 123 Wing Drive, Ithaca, NY 14853.*

Massimo Marchesi, *Ph.D., Postdoctoral Fellow in the Department of Civil and Environmental Engineering, University of Waterloo, Waterloo, ON, Canada. Now a Research Fellow at Politecnico di Milano, Dept. of Civil and Environmental Engineering, 32 Piazza L. Da Vinci, Milano, MI, Italy, 20133.*

Christopher M. DeRito, *M.S., is Research Support Specialist at Department of Microbiology, Cornell University, 125 Wing Drive, Ithaca, NY 14853.*

Daniel Bouchard, *Ph.D., Postdoctoral Fellow at Centre for Hydrogeology and Geothermics, University of Neuchatel, Neuchatel, Switzerland. Now at Sanexen Services Environnementaux Inc., 9935 Avenue de Châteauneuf, Bureau 200, Brossard, QC, Canada J4Z 3V4.*

Tim Buscheck, *M.Sc., is Chevron Fellow and Senior Consulting Hydrogeologist at Health, Environment, and Safety Department, Chevron Energy Technology Company, 6001 Bollinger Canyon Rd., San Ramon, CA 94583.*

Ravi Kolhatkar, *Ph.D., M.B.A., is Senior Staff Hydrogeologist at Health, Environment, and Safety Department, Chevron Energy Technology Company, 1200 Smith St., Houston, TX 77002.*

Eric J. Daniels, *Ph.D., is Consulting Hydrogeologist at Health, Environment, and Safety Department, Chevron Energy Technology Company, 6001 Bollinger Canyon Rd., San Ramon, CA 94583.*